# Electronic Tuning of Monolayer Graphene with Polymeric "Zwitterists"

James Nicolas Pagaduan,<sup>†</sup> Nicholas Hight-Huf,<sup>‡</sup> Avdhoot Datar,<sup>∥</sup> Yehiel Nagar,<sup>⊥</sup> Michael Barnes,<sup>‡</sup> Doron Naveh,<sup>⊥</sup> Ashwin Ramasubramaniam,<sup>\*∥</sup> Reika Katsumata,<sup>\*†</sup> and Todd Emrick<sup>\*†</sup>

†Polymer Science and Engineering Department, †Department of Chemistry, and †Department of Mechanical and Industrial Engineering, University of Massachusetts, Amherst, MA 01003, USA <sup>4</sup>Faculty of Engineering and Institute for Nanotechnology and Advanced Materials, Bar-Ilan University, Ramat-Gan 52900, Israel

### **Abstract**

Work function engineering of two-dimensional (2D) materials by application of polymer coatings represents a research thrust that promises to enhance performance of electronic devices. While polymer zwitterions have been demonstrated to significantly modify the work function of both metal electrodes and 2D materials due to their dipole-rich structure, the impact of zwitterion chemical structure on work function modulation is not well understood. To address this knowledge gap, we synthesized a series of sulfobetaine-based zwitterionic random copolymers with variable substituents and used them in lithographic patterning for the preparation of negative-tone resists (*i.e.*, "zwitterists") on monolayer graphene. Ultraviolet photoelectron spectroscopy indicated a significant work function reduction, as high as 1.5 eV, induced by all polymer zwitterions when applied as ultrathin films (< 10 nm) on monolayer graphene. Of the polymers studied, the piperidinyl-substituted version produced the largest dipole normal to the graphene sheet, thereby inducing the maximum work function reduction. Density functional theory calculations probed the influence of zwitterion composition on dipole orientation, while lithographic patterning allowed for evaluation of surface potential contrast *via* Kelvin probe force microscopy. Overall, this polymer "zwitterist" design holds promise for fine-tuning 2D materials electronics with spatial control based on the chemistry of the polymer coating and the dimensions of the lithographic patterning.

**Keywords:** graphene, sulfobetaine, doping, interface, zwitterion, photoresist

#### Introduction

Two-dimensional (2D) materials offer routes to fundamental advances in nanoscale devices due to their characteristic electronic properties. <sup>1,2</sup> In the case of graphene, which is already exceptionally interesting in its pristine form, an even broader range of properties becomes available *via* structural modification and/or contact with organic or inorganic materials (*i.e.*, as coatings). Through such methods, the fundamental electronic properties of 2D materials, such as work function (*i.e.*, the energy required to promote an electron from the Fermi level to vacuum), can be modulated to adjust band alignment, tune charge injection barriers, and control the charge carrier type and density. <sup>3,4</sup> For graphene, current approaches to work function engineering of this type include chemical doping by atomic insertion into the 2D structure, gas adsorption, electrostatic gating, and application of mechanical strain. <sup>5–9</sup> An alternative approach to modulate graphene electronics is by its contact with synthetic polymers, which is advantageous for the outstanding film-forming properties and rich chemical variation available with polymers. <sup>10–13</sup> Moreover, such hard-soft (*i.e.*, 2D material-polymer) interfaces enhance 2D materials properties, processing, and electronic function *via* the combination of polymeric chemical functionality with lithographic patterning methods.

Functional polymers are increasingly recognized for their ability to modulate the electronic properties of both metals and 2D materials. Herein, we examine polymer zwitterions, specifically, several derivatives of sulfobetaine (SB)-containing polymers, for their role in work function modulation of graphene. In prior

studies, we showed that thin films of zwitterionic polymers, containing pendent groups that serve as molecular dipoles, significantly alter the work function of metal electrodes and 2D materials.<sup>19–21</sup> Distinct from the effect of cationic or anionic polyelectrolytes on electronic substrates, the balanced charges of polymer zwitterions make them electrically neutral and thus devoid of mobile counter ions that may deteriorate long-term stability, prolong response time, and complicate device operation mechanisms.<sup>22–25</sup> Notably, the selective solubility of polymer zwitterions is additionally advantageous for its orthogonality to the solubility of other polymer/interfacial layers, thus enabling facile deposition as thin films in layer-by-layer approaches.<sup>26</sup> Moreover, the interest in polymer zwitterions for electronics is growing rapidly, as seen in recent examples using poly(sulfobetaine methacrylate) (PSBMA) as both dopant and trap passivation layer, with resultant improved performance of organic light-emitting diodes (OLEDs) and solar cells.<sup>27–29</sup>

Our recent work on hard-soft interfaces involving copolymers of SBMA and methyl methacrylate (MMA) produced positive-tone electron beam resists on graphene/SiO<sub>2</sub>/Si with an observed shift in the charge neutrality point attributed to a localized, non-covalent surface doping.<sup>30</sup> In explaining these findings, density functional theory (DFT) calculations pointed to a zwitterion orientation that produced a net dipole moment of 4.7 Debye (D) normal to graphene. These results prompted us to examine how zwitterion chemical structure impacts the electronic properties of the contacting graphene, as described here *via* a combination of synthesis, computation, and electronic characterization. Such fundamental understanding is important for advancing the role of polymers in modifying 2D materials properties and ultimately providing materials combinations for enhancing device performance.<sup>31,32</sup>

This study probes the influence of a series of SB-containing polymer films on the electronic properties of graphene, utilizing ultraviolet photoelectron spectroscopy (UPS), Kelvin probe force microscopy (KPFM), and DFT calculations. Use of a polymer coating effectively alters the 2D surface potential while maintaining the fundamental structural characteristics of graphene (i.e., avoiding the need to directly modify graphene). The work function shift,  $\Delta \phi$ , of polymer-coated graphene, relative to graphene itself, is expressed as  $\Delta \phi = -qD/\epsilon_0 \epsilon_{eff}$ , where  $D = \rho \mu_{\perp}$  is the dipole moment per unit area,  $\rho$  is the area density of dipoles,  $\mu_{\perp}$  is the component of the dipole oriented normal to graphene, and  $\varepsilon_{eff}$  is the effective dielectric constant of the embedding medium. Thus,  $\Delta \phi$  of the 2D structure can in principle be adjusted by varying the orientation ( $\theta$ ) of the dipole relative to the graphene sheet and thus, the magnitude of  $\mu_1$ , potentially imparted by appropriate modification of zwitterion structure (Figure 1a,b). As shown in Figure 1c, Nsubstituted PSBMA copolymers (abbreviated **PxSBMA**, where x denotes the N-substituents as R and R' groups) were prepared. Using MMA as a co-monomer enhanced thin film formation, while inclusion of benzophenone methacrylamide (BPMA) contributed cross-linking capabilities characteristic of negativetone resists. UPS measurements enabled comparison of the work function of bare graphene vs. the zwitterion-coated samples, while first-principles DFT calculations provided theoretical insights into zwitterion configuration on graphene, and the resultant  $\mu_{\perp}$  and  $\Delta\phi_{DFT}$  values. Successful lithographic patterning of zwitterists was confirmed by topography measurements obtained through KPFM, which also revealed spatially dependent surface potential distributions on bare and polymer-coated graphene. Overall, this method of work function engineering permits scalable lithographic patterning of polymer zwitterion films, and by extension control over carrier doping, that is valuable for developing the field of monolayer graphene-based devices.

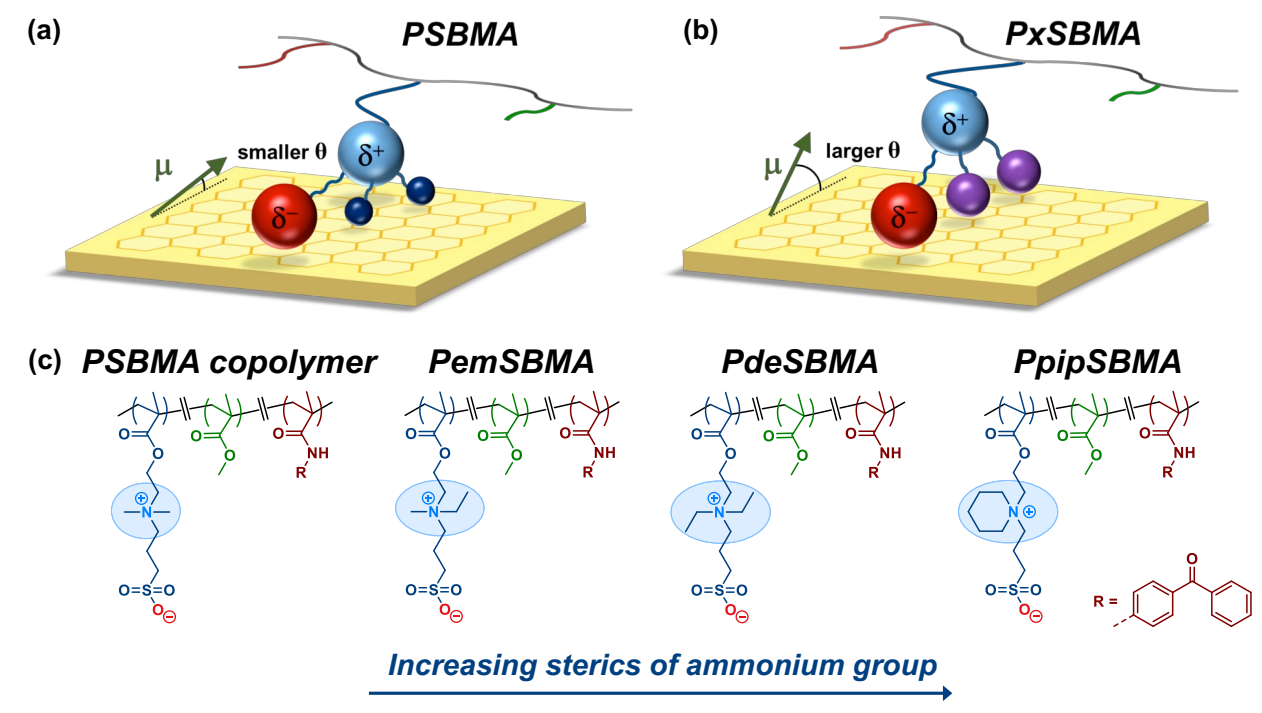
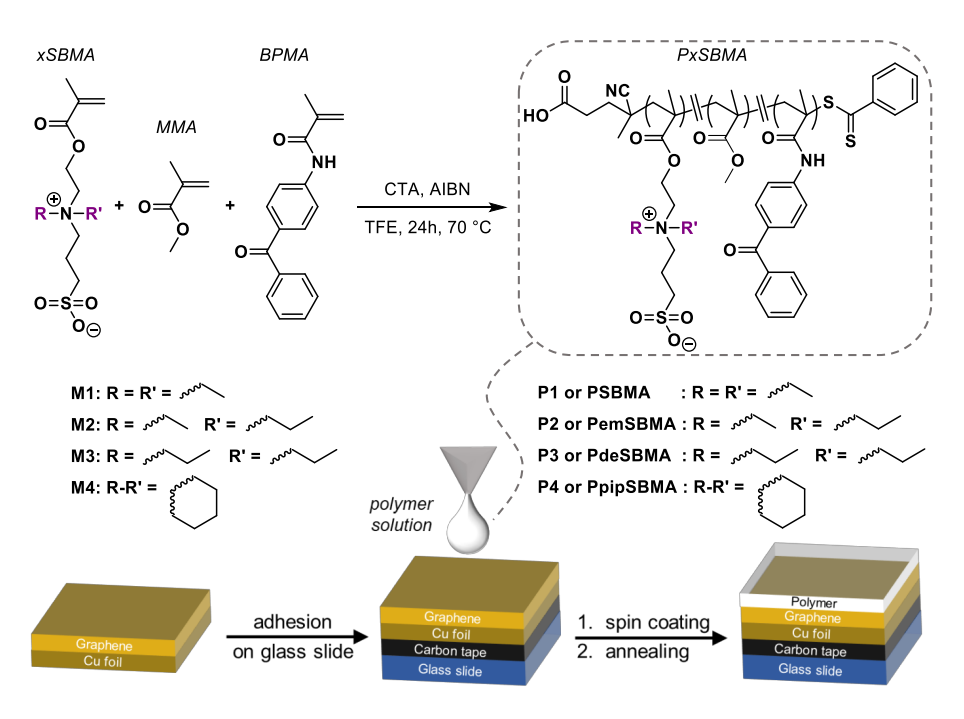


**Figure 1**. (a) Illustration of poly(sulfobetaine methacrylate) (PSBMA) on monolayer graphene, showing the dipole moment  $\mu$  and dipole orientation  $\theta$ ; (b) illustration of modulating  $\theta$  by selection of ammonium substituents (nitrogen, sulfonium, methyl, and "steric" groups are indicated by light blue, red, dark blue, and purple spheres, respectively); and (c) copolymer structures with increasing steric footprint of the ammonium group: "em" = ethyl/methyl, "de" = diethyl; "pip" = piperidinyl.

### **Results and Discussion**

Polymer synthesis and work function characterization. As illustrated in Scheme 1, polymer zwitterions P1-P4 were prepared by controlled free radical polymerization of the corresponding sulfobetaine methacrylate monomers M1-M4. The zwitterionic monomer syntheses hinge on the reaction of aminoalkyl-substituted methacrylates with 1,3-propanesultone, each conducted with slight modification of published procedures<sup>33–35</sup> to afford white powders of ethylmethyl-SBMA (M2), diethyl-SBMA (M3), and piperidinyl-SBMA (M4). The steric footprints of the R/R' substituents increase as methyl/methyl < ethyl/methyl (em) < diethyl (de) < piperidinyl (pip) (SBMA (M1) is available commercially). The zwitterionic monomers were copolymerized with MMA and BPMA by reversible addition-fragmentation chain transfer (RAFT) polymerization at 70 °C in a 2,2,2-trifluoroethanol (TFE) solution containing a dithiobenzoate chain transfer agent and an azo-initiator. This afforded the desired polymers as light pink solids with estimated number-average molecular weight (M<sub>n</sub>) values in the 21-29 kDa range and PDI values of 1.1-1.3. PMMA and P(MMA-co-BPMA), each lacking the zwitterionic components, were also synthesized for comparative evaluation. The polymers were applied to monolayer graphene (grown on copper foil in 10 mm x 10 mm dimensions) by spin-coating from TFE solutions at 4000 rpm. The foil was initially adhered on a glass slide, as illustrated in Scheme 1, to facilitate processing and characterization. By adjusting the polymer concentration in TFE from 0.1-1 mg/mL, polymer films of 1-8 nm thickness on graphene were formed, judging from ellipsometry characterization of polymer-coated Si prepared similarly (Figure S13). Step-height profiles from atomic force microscopy (AFM) measurements (Figure S22), performed on polymer zwitterion-coated graphene, revealed polymer layers of ~1-7 nm thickness, in agreement with the ellipsometric measurements.



**Scheme 1**. Synthesis of sulfobetaine-containing polymer zwitterions by RAFT polymerization with variation of R and R' groups (top); preparation of polymer-coated graphene for electronic tuning and characterization (bottom).

The work function of polymer-coated graphene, using the sample configuration shown in **Scheme 1**, was measured by UPS, which allows determination of electronic levels in the valence band by quantifying the kinetic energy of emitted photoelectrons following vacuum UV absorption.<sup>36</sup> The reported work function values represent the energy difference between the incident photons (21.2 eV for He I radiation) and that corresponding to the secondary electron cut-off of the spectrum. For bare graphene on Cu(111) foil (i.e., Gr/Cu), a work function of 4.65 eV was measured, in accord with literature values. <sup>37–39</sup> As shown in **Figure** 2a, all of the polymer-coated graphene samples produced lower work function values relative to bare Gr/Cu, corresponding to an *n*-doping of graphene; the quantitative extent of work function reduction represents, by definition, the interfacial dipole energy. PMMA, having a small molecular dipole (1.7 D) associated with the carbonyl group,  $^{40,41}$  produced the smallest  $\Delta\phi$  (~0.1 eV for nominally 1-nm films and nearing 1 eV for 7-nm films). PMMA containing small mole percentages of BPMA to effect cross-linking produced similar results (data not shown). In contrast, coatings of the copolymers, in which about half of the MMA units are replaced with zwitterions, produced much more extensive work function reduction, from 0.5-1.0 eV for 1-2 nm films to nearly 1.5 eV at ~4 nm film thickness, depending on the polymer employed. At coating thicknesses of 4 nm and beyond, the work function reduction plateaued. With the anionic component of sulfobetaine pointing towards graphene, a negative  $\Delta \phi$  is anticipated due to a decrease of the vacuum level energy; this is illustrated in Figure 2b and described further in prior work on polymer zwitterion-coated metals<sup>42</sup> and organic/metal interfaces.<sup>43</sup>

While the polymer zwitterions with different R-substituents yielded relatively similar profiles in work function reduction with film thickness, the reduction caused by the piperidinyl-containing structure was more pronounced, especially for thinner films (noting a ~0.25 eV difference for the 2-nm films). Notably, greater work function reduction was observed with increasing polymer film thickness, which provides a mechanism for tuning electronic properties as desired for a given application. This observed impact of film thickness is attributed to several potential factors, including 1) a reduction in the likelihood of coating imperfections or pinholes at the polymer-graphene interface of smaller size-scale than the AFM tip and 2) electron energy loss associated with the work done by an electron when passing through the polymer layer.

Additional contributions from stacked dipoles, involving multiple zwitterion layers, cannot be ruled out though we do not have evidence for such a structure at present. Such saturation of work function reduction has also been observed for polymer-coated metals<sup>44,45</sup> and metal substrates coated with organic molecules such as tetrafluoro-tetracyanoquinodimethane (F4-TCNQ) and C<sub>60</sub>-fullerene.<sup>46,47</sup> We should note that the effect of PMMA on work function reduction, though not as large as that of the polymer zwitterions, is significant and likely due to a "push-back" effect<sup>48–51</sup> associated with van der Waals interactions, and warrants further theoretical and experimental/mechanistic study.

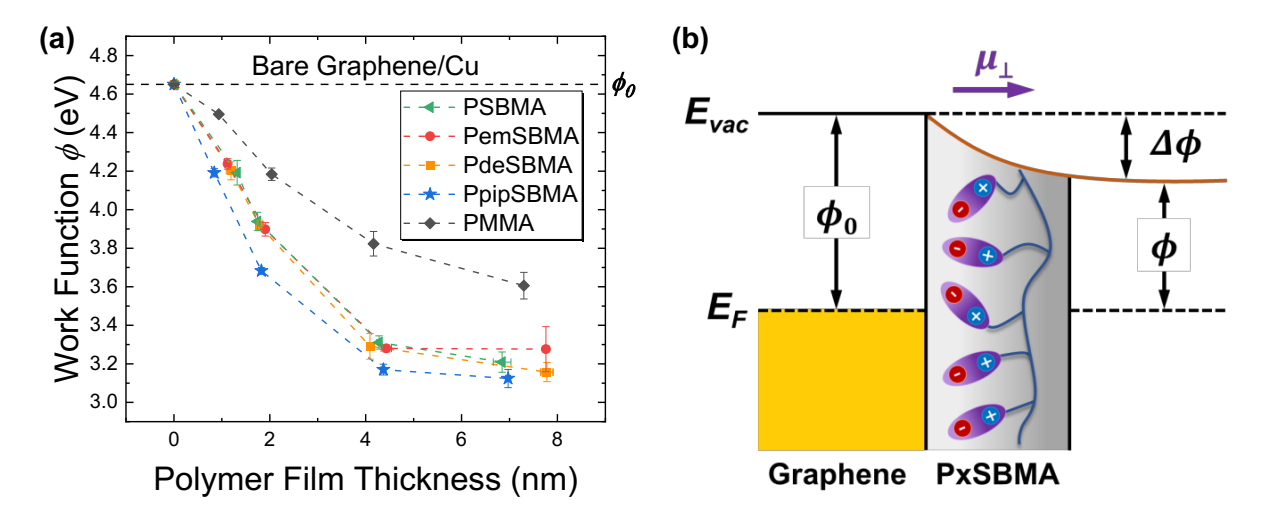


**Figure 2.** (a) Comparison of work function  $\phi$  of PMMA- and zwitterionic polymer-coated graphene measured by UPS (mean  $\pm$ s.d. of  $n \ge 3$  replicates); (b) illustration of interface dipole induced by graphene-polymer contact (orange curve in the upper-right reflects the impact of film thickness on work function reduction).

Density functional theory calculations. First-principles density functional theory (DFT) calculations were performed to gain microscopic insights into graphene/zwitterion interactions. As in our prior work, 30 the DFT calculations employed the key components of the system, namely the zwitterionic moiety and a graphene sheet supported on a Cu(111) slab (Gr/Cu slab). The two limiting cases of zwitterion adsorption configurations, flat and standing, are illustrated in Figure 3b,c. The flat dipole orientation is favored, since attractive dispersion interactions with the Gr/Cu slabs are maximized, while the standing configuration corresponds to a higher energy local minimum, (i.e., is statistically less likely to be observed (Figure 4)). For the flat configuration, only a small component of the zwitterion dipole moment is normal to the Gr/Cu slab, 30 resulting in a smaller  $\Delta \phi_{DFT}$  (lower bound). The standing configuration, in contrast, displays the largest possible  $\mu_{\perp}$  and thus the largest  $\Delta\phi_{DFT}$  (upper bound). Any orientational anisotropy in adsorption configurations of the pendent groups is captured within these two bounds. Specifically, for SBMA, the flat and standing configurations exhibited  $\mu_{\perp}$  values of 5.15 D and 12.74 D, respectively. We note that the net dipole moments reported here account for the dipole of the zwitterionic moiety as well as the interfacial graphene-Cu dipole. To determine  $\Delta \phi_{DFT}$  values, we first consider that the calculated work function of a freestanding monolayer graphene is 4.24 eV, which is altered to 4.16 eV when adsorbed on a Cu(111) surface (Figure 3d) due to both charge transfer from Cu to Gr and Gr-Cu chemical interactions.<sup>52</sup> Adsorption of a flat SBMA moiety results in a modified work function of 3.54 eV (Figure 3e), while the standing moiety alters the work function to 1.75 eV (Figure 3f). Thus, relative to the bare Gr/Cu slab, the flat and standing SBMA moieties reduce the work function of the Gr/Cu slab by 0.62 eV and 2.41 eV, respectively.

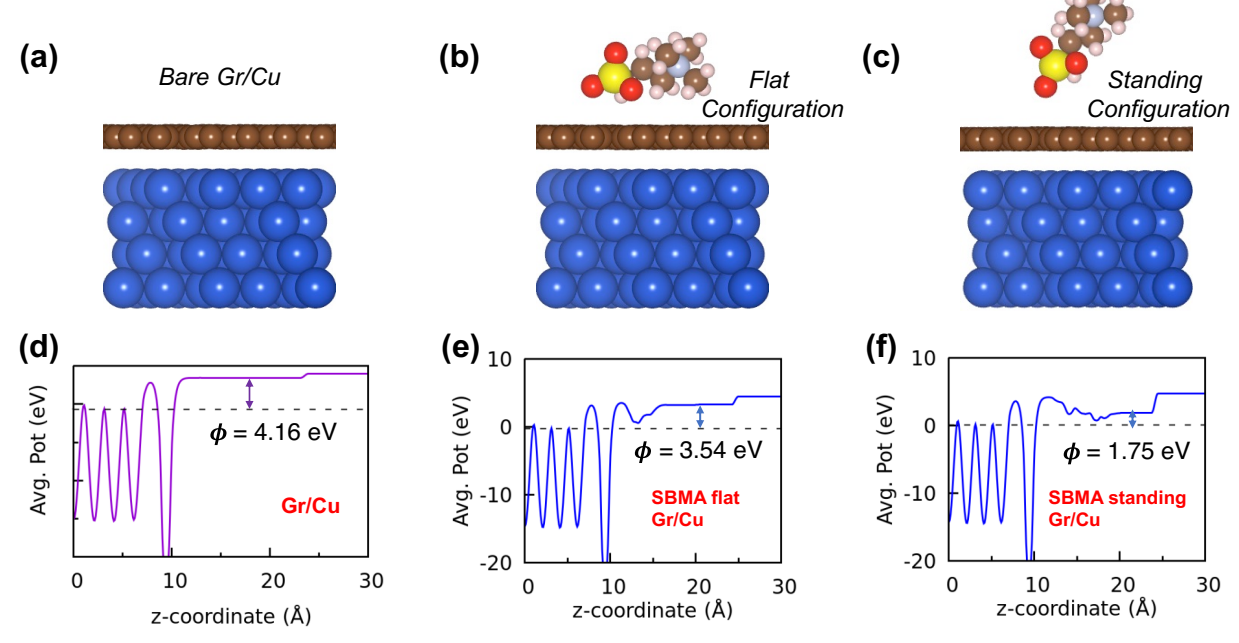


**Figure 3.** Optimized DFT structures of (a) bare graphene on Cu(111) slab (Gr/Cu) and SBMA moieties adsorbed in (b) flat and (c) standing orientations on Gr/Cu. Planar-averaged potentials of (d) Gr/Cu, (e) flat SBMA moiety on Gr/Cu, and (f) standing SBMA moiety on Gr/Cu. Fermi levels (dashed lines) and the distance to the vacuum level (*i.e.*, the work function) are indicated in each case.

The zwitterions adsorbed on Gr/Cu slabs display different ranges of work function shifts  $\Delta\phi_{DFT}$  and values of the dipole moment normal to graphene  $\mu_{\perp}$ , as summarized in **Figure 4**, which also indicates the relative energies,  $\Delta E$ , between the illustrated standing and flat configurations (positive  $\Delta E$  values indicate favorability of flat configurations). The SBMA, emSBMA, and deSBMA moieties induce relatively similar  $\Delta\phi_{DFT}$  (0.57 to 0.75 eV) when adsorbed in their most favorable flat orientations, which is qualitatively consistent with UPS measurements. The pipSBMA moiety induces a much larger work function shift of nearly 1.2 eV in its most stable (flat) orientation, a finding qualitatively consistent with UPS results. By examining the optimized DFT structures, the larger steric footprint of the piperidinyl moiety in its favorable flat configuration appears to push the positively charged end of the dipole (quaternary ammonium cation NR<sub>4</sub><sup>+</sup>) further away from the Gr/Cu surface, leading to a larger  $\mu_{\perp}$  (7.45 D). This larger dipole moment, in turn, induces a greater  $\Delta\phi_{DFT}$ . It is worth noting that the DFT calculations show negligible charge transfer between the studied zwitterionic moieties and Gr/Cu slab (or even freestanding graphene, see **Figure S27-28**), indicating that the work function shifts are essentially caused by the adsorbed dipoles and can potentially be controlled by manipulating dipole orientation  $\theta$ .

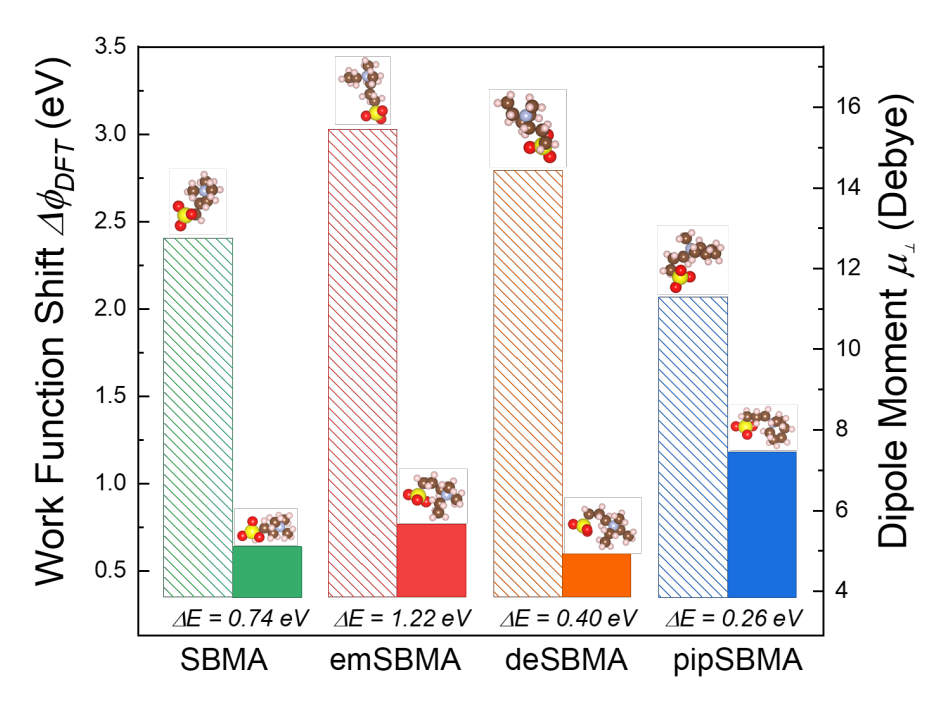


**Figure 4.** Calculated maxima and minima of  $\Delta \phi_{DFT}$  (relative to bare Gr/Cu slab with  $\phi = 4.16$  eV) and component of dipole moment normal to graphene  $\mu_{\perp}$  corresponding to the standing (hatched bars) and flat (solid bars) orientations of adsorbed zwitterions. The energy difference,  $\Delta E$ , between standing and flat configurations is indicated, with positive values signifying the lower stability of the standing configurations in all cases.

Lithographic patterning and Kelvin probe force microscopy measurements. The impact of lithographic patterning of zwitterionic polymer films on Gr/Cu, and the associated surface potential contrast (SPC) variation across the patterned samples, was investigated using Kelvin probe force microscopy (KPFM). The photoactive BPMA comonomers enable production of negative-tone resists in which the exposed regions are amenable to UV-induced crosslinking.<sup>53,54</sup> Figure 5a illustrates an example of the photolithographic process used for preparing a zwitterist from P4 on Gr/Cu, which was achieved by UV irradiation at 365 nm through a photomask, followed by developing in TFE to remove uncrosslinked regions, and drying under a stream of  $N_{2(g)}$ . Uniform rectangular 120-micron wide stripes of polymer were obtained on Gr/Cu, as shown in Figure 5b; similar control samples were also prepared on Gr/SiO<sub>2</sub>/Si (Figure S30). In dual-pass KPFM, surface topography was acquired in the first pass followed by the surface potential measurement in the second pass, as depicted in Figure 5c-e. The SPC profile presented was obtained following calibration of the work function of the AFM tip using freshly cleaved highly oriented pyrolytic graphite (HOPG) as a reference. The height profiles in Figure 5c, e indicate the patterned polymers to be ~10 nm in thickness. The onset of change in SPC is evident near the interfacial area indicated by the topographic profile (Figure 5d and e). The observed increase in SPC in the zwitterioncoated regions, relative to bare Gr/Cu, is shown in Figure 5f, corresponding to a work function reduction that is qualitatively consistent, though smaller in magnitude, with the n-type doping of graphene seen in UPS measurements. In unpatterned polymer-coated graphene samples,  $\Delta\phi_{KPFM}$  values of -0.20 eV and -0.47 eV were obtained for the PSBMA- and PdeSBMA-coated samples, respectively (Figure S31). The current-voltage (I-V) transfer curves of field effect devices, prepared using bare and PpipSBMA-coated graphene, are shown in **Figure S32**. Bare graphene had a hole density of  $3 \times 10^{11}$  cm<sup>-2</sup>, attributed to ambient humidity, while the polymer-coated devices had an electron density of  $2.2 \times 10^{12}$  cm<sup>-2</sup>, which further confirmed n-type doping of graphene by the polymer layer, with a corresponding work function shift of ~0.24 eV. A half-covered device produced a signature p-n homojunction curve, in which the observed double minima results from the combined I-V curves of the bare and polymer-coated structures. We anticipate that this demonstration of SPC variation and  $\Delta \phi$  across a patterned negative-tone functional photoresist-type structure will be useful for work function engineering of electronic devices.

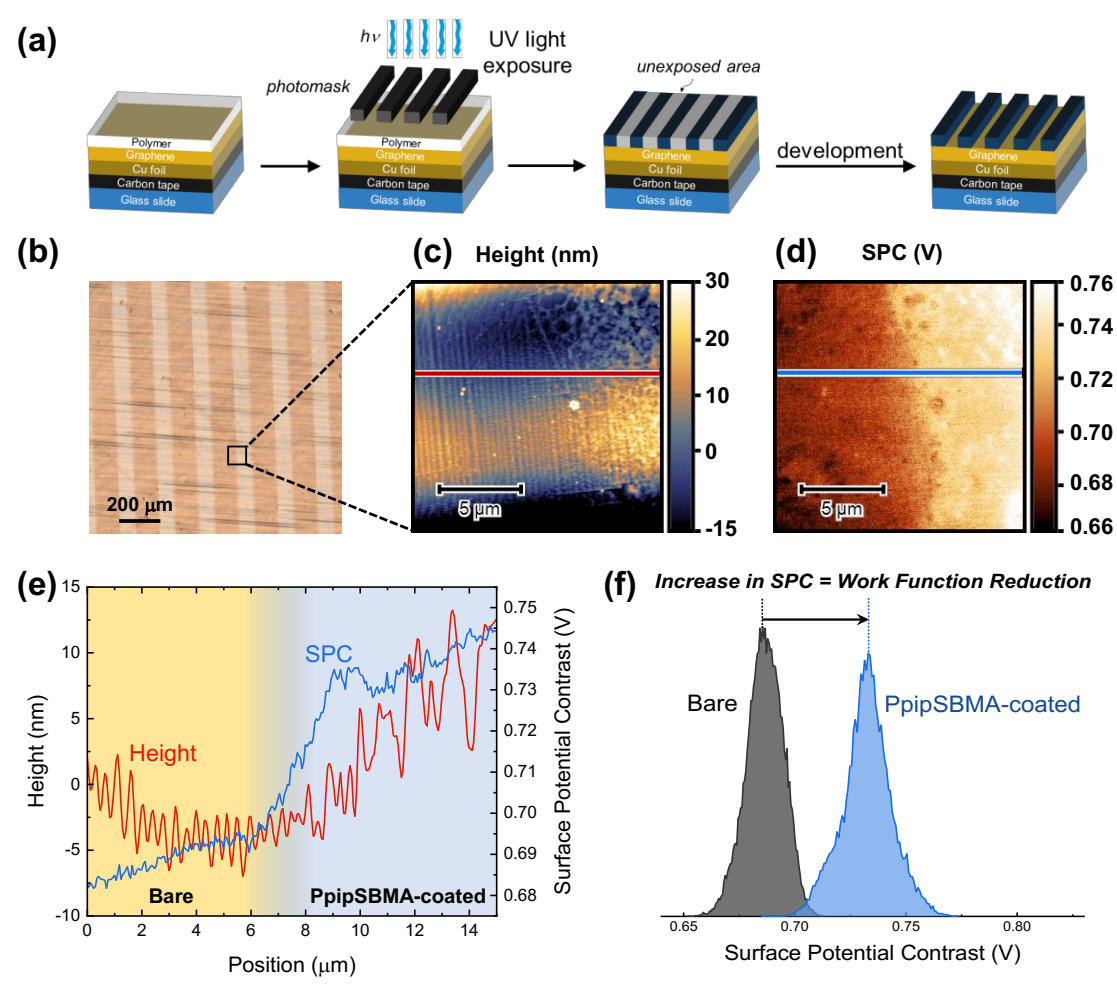


**Figure 5**. (a) Schematic diagram of the preparation of polymer zwitterists on graphene/Cu substrate *via* UV lithography and (b) corresponding optical image of patterned PpipSBMA film. Kelvin probe force microscopy of PpipSBMA on graphene/Cu substrate showing the (c) height and (d) surface potential contrast (SPC) images with corresponding (e) line profiles, and (f) normalized SPC distributions of bare and polymer-coated regions.

### **Conclusions**

To summarize, the electronic sensitivity of monolayer graphene to its proximate environment was leveraged using a simple, solution-based coating of graphene with substituted zwitterionic copolymers. UPS measurements revealed a work function reduction of graphene owing to contact with the polymer zwitterion (corresponding to *n*-type doping), with a distinct influence of polymer film thickness on extent of work function reduction. This experimental finding is supported by theoretical insight derived from DFT calculations that probed the energetics of zwitterion orientation on graphene. KPFM measurements confirmed successful photolithographic patterning of negative-tone "zwitterists", with an associated increase in SPC (*i.e.*, reduction in work function) with respect to bare graphene corresponding to the patterns. The combination of functional polymers, solution processing, and patterning methods for graphene

modification established in this study are anticipated to be readily applicable to electronic devices requiring spatial control over work function modulation.

#### Methods

Materials. [2-(Methacryloyloxy)ethyl]dimethyl-(3-sulfopropyl)ammonium hydroxide (SBMA), methyl methacrylate (MMA, 99%), methacryloyl chloride (97%), 1,3-propanesultone (98%), 4-methoxyphenol (99%), 4-aminobenzophenone, 2,2'-azobisisobutyronitrile (AIBN, 98%), 4-cyano-4-(phenylcarbonothioylthio)pentanoic acid, triethylamine (TEA, 99.0+%), acetonitrile (99.8%), and dichloromethane (DCM, 99.8+%) were purchased from Sigma-Aldrich (St. Louis, MO, USA). 2-(Diethylamino)ethyl methacrylate (98.5+%), 2-(methylamino)ethanol (99.0+%), and iodoethane (99.0+%) were obtained from TCI Chemical (Portland, OR, USA). 2-Piperidinoethanol (99%) and butylated hydroxytoluene (BHT, 99%) were purchased from Alfa Aesar (Haverhill, MA, USA). Chemical vapor deposition (CVD)-grown monolayer graphene on copper foil (25-µm thick) and monolayer graphene transferred onto Si/SiO<sub>2</sub> wafer were obtained from Grolltex, Inc (San Diego, CA, USA). Chloroform-d (99.8%), deuterium oxide (99.9%), 2,2,2-trifluoroethanol-d3 (99%) were purchased from Cambridge Isotope Laboratories (Tewksbury, MA, USA). Diethyl ether, methanol, sodium hydroxide (NaOH, 97.0+%), hydrochloric acid (HCl, 36.5 to 38.0% w/w), sodium bicarbonate (NaHCO<sub>3</sub>), sodium chloride (NaCl), and anhydrous magnesium sulfate (MgSO<sub>4</sub>) were purchased from Fisher Scientific (Waltham, MA, USA). TFE (99.9%) was obtained from Oakwood Products, Inc (West Columbia, SC, USA). Before use, MMA was run through a plug of basic alumina to remove the inhibitor, and AIBN was recrystallized from methanol. TEA and DCM were separately dried and distilled over calcium hydride. All other materials were used as received without additional purification.

Polymer Synthesis and Characterization. Copolymers of sulfobetaine compound, MMA and BPMA were prepared by reversible addition—fragmentation chain-transfer polymerization as shown in **Scheme 1**. The chain transfer agent 4-cyano-4-(phenylcarbonothioylthio)pentanoic acid, 2,2'-azobisisobutyronitrile initiator ([CTA]:[AIBN] = 1:0.3), sulfobetaine monomer (50 eq.), MMA (47 eq.), BPMA (3 eq.) and TFE were mixed in a 20 mL vial equipped with a magnetic stir bar and rubber septum. The reaction mixture was degassed using dry nitrogen gas for 30 min and then stirred at 70 °C for 24 h. The polymerization was quenched by rapidly cooling the solution in liquid nitrogen and opening to air. The crude product was diluted with TFE and precipitated in methanol. To remove the remaining monomer, dialysis in 300 mM NaCl aqueous solution and pure water was performed. Subsequent freeze-drying afforded the solid polymer product. PMMA and P(MMA-BPMA) were synthesized following similar procedures but were purified by precipitation into methanol (rather than by dialysis and lyophilization). <sup>1</sup>H NMR (500 MHz) spectra of the polymer products were recorded on a Bruker Ascend<sup>TM</sup> 500 spectrometer equipped with a Prodigy cryoprobe. Gel permeation chromatography (GPC, using PMMA calibration standards) was conducted using an eluent mixture of TFE with 0.02 M sodium trifluoroacetate at 40 °C on an Agilent 1200 system equipped with the following: an isocratic pump operated at 1 mL/min, a degasser, an autosampler, one 50 mm × 8 mm PSS PFG guard column (Polymer Standards Service), and three 300 mm × 7.5 mm PSS PFG analytical linear M columns with 7 µm particle size (Polymer Standards Service), and an Agilent 1200 refractive index detector.

**Sample Preparation.** CVD-grown monolayer graphene on copper foil (10 mm × 10 mm) was adhered to a microscope slide using high-vacuum double-sided adhesive carbon tape, as shown in **Scheme 1**. Solutions of PSBMA and its derivatives in TFE with varying concentrations, from 0.1 to 1 mg/mL, were individually

spin-coated onto these substrates at 500 rpm for 5 s and then at 4000 rpm for 55 s. Prior to deposition, the polymer solutions were subjected to sonication (inserting a glass vial of the polymer solution into a sonication bath) for 10 minutes at room temperature and filtered through a PTFE membrane (0.2  $\mu$ m VWR). To remove residual solvent, samples were dried under vacuum at 65 °C overnight prior to UPS characterization. The polymer films were crosslinked by UV irradiation ( $\lambda = 365$  nm) with a dose of 20000 mJ cm<sup>-2</sup> through a quartz photomask. The samples were soaked in TFE for 10 s to remove the uncrosslinked regions and dried with a nitrogen gun, affording patterned resists which were measured *via* KPFM.

**Polymer Film Thickness Measurement.** The same polymer solutions as described above, with varying concentrations, were separately spin-coated on Si substrates at 500 rpm for 5 s and then 4000 rpm for 55 s. Si wafers were cleaned by washing with acetone, 2-propanol, and deionized water in a benchtop sonication bath, then dried under a flow of  $N_{2(g)}$  and subjected to 15 min of UV-ozone treatment with UVO-Cleaner® Model 18 (Jelight Company, Inc.). Ellipsometric measurements were made with a Gaertner LSE stokes ellipsometer equipped with a 632.8 nm Helium-Neon (HeNe) laser at a fixed angle of incidence from the normal to the plane of 70 °. Five to seven measurements were performed on a single substrate at different spots and averaged; film thickness was calculated using Gaertner Ellipsometer Measurement Program (GEMP) software from the ellipsometric parameters  $\Delta$  and  $\Psi$ . Uncoated Si wafers were also examined to determine the thickness of the native oxide layer (assuming a refractive index of 1.46 for the silica layer).

**Ultraviolet Photoelectron Spectroscopy (UPS) Measurement.** UPS spectra were collected with the Electron Spectroscopy for Chemical Analysis instrument (Scienta Omicron Nanotechnology, model ESCA+S) at a base pressure of  $4\times10^{-8}$  mbar. The instrument configuration consisted of a He discharge lamp (He I line, 21.2 eV) as the UV excitation source and a hemispherical SPHERA energy analyzer. The measurements were performed at a -3 V sample bias to collect the low kinetic energy electrons. The binding energy scale in the UPS spectra is given with reference to a vacuum level, which was taken as 21.2 eV away from the onset of the secondary electron cut-off energy.

KPFM and AFM Measurements. KPFM data were collected on a Digital Instruments Bioscope AFM/KPFM in two-pass lift mode under ambient atmospheric conditions (22 °C, 45% RH). The AFM probes were platinum-coated silicon (ANSCM-PT) with f<sub>0</sub> of ~70 kHz, used as supplied by App Nano. Samples were grounded using silver paint from Electron Microscopy Sciences. To monitor changes in the surface potential of the polymer-coated and bare monolayer graphene on copper foil, KPFM was performed on the same samples measured by UPS. The height and phase profiles of the zwitterionic copolymer films on graphene were evaluated by AFM using an MFP-3D instrument (Oxford Instruments Asylum Research, Inc.) in tapping mode under ambient conditions. The profiles were analyzed using the scanning probe microscopy data analysis software Gwyddion.

Computational Data. Density functional theory (DFT) calculations were performed using the Vienna *ab Initio* Simulation Package (VASP).<sup>55,56</sup> The core and valence electrons were represented using the projector-augmented wave method <sup>56,57</sup> and the Perdew–Burke–Ernzerhof generalized-gradient approximation was used to describe electron exchange and correlation.<sup>58</sup> The zero-damping DFT D3 method of Grimme *et al.*<sup>59</sup> was used to model dispersion interactions. Based on convergence studies, the kinetic energy cutoff was set to 400 eV and a Gaussian smearing of 0.05 eV was used for Brillouin-zone integrations. Using the conjugate-gradient method, atomic positions were optimized with a force tolerance of 0.02 eV/Å. Slab

models for graphene monolayers on Cu slabs were generated using the CellMatch program; <sup>60</sup> the supercell was chosen to minimize the mismatch strain (0.58%) in the graphene sheet while keeping the computations tractable. The Cu slab was modeled using four layers of which the two bottommost ones were frozen at their bulk atomic positions; the two upper layers of the Cu slab and the adsorbed graphene sheet were fully relaxed in all calculations. To avoid spurious interactions between periodic images, at least 15 Å of vacuum was inserted normal to the slabs. Dipole corrections were applied in all calculations along the direction normal to the Gr/Cu slabs. <sup>61,62</sup> PSBMA-based pendants on freestanding graphene were studied using  $6\times6$  supercells. All relaxations were performed using  $3\times3\times1$   $\Gamma$ -centered k-point meshes. After relaxation, single-point electronic-structure calculations were performed using  $11\times11\times1$   $\Gamma$ -centered k-point meshes for Cu-supported graphene and  $13\times13\times1$   $\Gamma$ -centered k-point meshes for freestanding graphene.

**Device Fabrication.** CVD-grown graphene was transferred to a Si/SiO<sub>2</sub> substrate (~90 nm oxide layer). The electrodes were patterned by electron-beam lithography (EBL) followed by oxygen plasma for etching or electron-beam deposition for contact metallization. To pattern the polymer, a 4 mg/mL solution of PpipSBMA in TFE was deposited on the substrate by spin-coating at 500 rpm for 5 seconds, then at 3000 rpm for 45 seconds. The samples were baked at 150 °C for 3 min. The polymer film was exposed to a 5 kV e-beam with a dosage of 3000  $\mu$ C/cm<sup>2</sup>, baked at 150 °C for 1 min, and developed in distilled water for 10 seconds. The resultant chips were soaked in isopropanol for 30 s and dried under N<sub>2(g)</sub>.

## **Supporting Information**

Synthetic methods and characterization of the monomers and polymers; ellipsometry data; UPS spectra; AFM, KPFM, and optical images; supplementary DFT calculations; and electrical transport measurements.

### **Corresponding Author**

\*E-mail: tsemrick@mail.pse.umass.edu, rkatsumata@umass.edu, ashwin@engin.umass.edu

#### **Author Contributions**

All of the authors contributed to the preparation of this manuscript. J.N.P., R.K., and T.E. synthesized and characterized the monomers and polymers, prepared samples, and performed UPS measurements. N.H. and M.B. performed KPFM measurements. A.D. and A.R. conducted the computational analysis. D.N. and Y.N. performed the device fabrication and measurements.

#### **Notes**

The authors declare no competing financial interests.

## Acknowledgements

A.R., M.B., and T.E. gratefully acknowledge the National Science Foundation for support (NSF-BSF 1808011). D.N. acknowledges support from the BSF (2017655). UPS measurements were carried out in the Center for Electronic Materials and Devices, a core research facility at UMass Amherst, with the assistance of Dr. Volodimyr Duzhko. We also thank Dr. Keith Dusoe for assistance with AFM characterization. J.N.P. thanks PPG Industries, Inc. for the 2018-2019 PPG Foundation Fellowship. R.K. expresses gratitude for startup funding from UMass Amherst. A.D. and A.R. acknowledge computational support from the Extreme Science and Engineering Discovery Environment (XSEDE), which is supported by National Science Foundation grant number ACI-1548562.

#### References

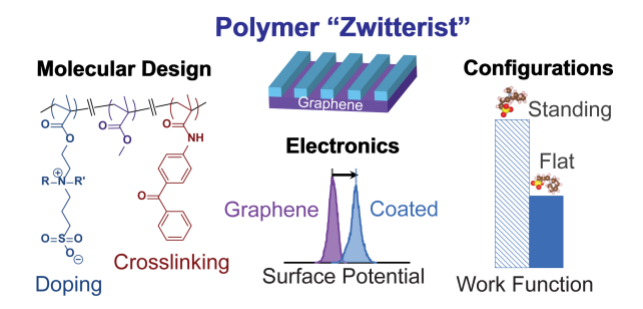
- (1) Briggs, N.; Subramanian, S.; Lin, Z.; Li, X.; Zhang, X.; Zhang, K.; Xiao, K.; Geohegan, D.; Wallace, R.; Chen, L.-Q.; Terrones, M.; Ebrahimi, A.; Das, S.; Redwing, J.; Hinkle, C.; Momeni, K.; Duin, A. van; Crespi, V.; Kar, S.; Robinson, J. A. A Roadmap for Electronic Grade 2D Materials. *2D Mater.* **2019**, *6* (2), 022001.
- (2) Vitiello, M. S. Nanodevices at Terahertz Frequency Based on 2D Materials. *J. Phys. Mater.* **2019**, *3* (1), 014008.
- (3) Garg, R.; Dutta, N. K.; Choudhury, N. R. Work Function Engineering of Graphene. *Nanomaterials* **2014**, *4* (2), 267–300.
- (4) Eda, G.; Emrah Unalan, H.; Rupesinghe, N.; Amaratunga, G. A. J.; Chhowalla, M. Field Emission from Graphene Based Composite Thin Films. *Appl. Phys. Lett.* **2008**, *93* (23), 233502.
- (5) Lee, J.; Novoselov, K. S.; Shin, H. S. Interaction between Metal and Graphene: Dependence on the Layer Number of Graphene. *ACS Nano* **2011**, *5* (1), 608–612.
- (6) Yu, Y.-J.; Zhao, Y.; Ryu, S.; Brus, L. E.; Kim, K. S.; Kim, P. Tuning the Graphene Work Function by Electric Field Effect. *Nano Lett.* **2009**, *9* (10), 3430–3434.
- (7) Gui, G.; Li, J.; Zhong, J. Band Structure Engineering of Graphene by Strain: First-Principles Calculations. *Phys. Rev. B* **2008**, *78* (7), 075435.
- (8) Zhang, Z.; Huang, H.; Yang, X.; Zang, L. Tailoring Electronic Properties of Graphene by π–π Stacking with Aromatic Molecules. *J. Phys. Chem. Lett.* **2011**, *2* (22), 2897–2905.
- (9) Kumar Singh, A.; Waqas Iqbal, M.; Kumar Singh, V.; Zahir Iqbal, M.; Hong Lee, J.; Chun, S.-H.; Shin, K.; Eom, J. Molecular *n*-Doping of Chemical Vapor Deposition Grown Graphene. *Journal of Materials Chemistry* **2012**, *22* (30), 15168–15174.
- (10) Selhorst, R. C.; Puodziukynaite, E.; Dewey, J. A.; Wang, P.; Barnes, M. D.; Ramasubramaniam, A.; Emrick, T. Tetrathiafulvalene-Containing Polymers for Simultaneous Non-Covalent Modification and Electronic Modulation of MoS<sub>2</sub> Nanomaterials. *Chem. Sci.* **2016**, *7* (7), 4698–4705.
- (11) Selhorst, R.; Wang, P.; Barnes, M.; Emrick, T. Bithiazolidinylidene Polymers: Synthesis and Electronic Interactions with Transition Metal Dichalcogenides. *Chem. Sci.* **2018**, *9* (22), 5047–5051.
- (12) Li, H.; Su, S.; Liang, C.; Zhang, T.; An, X.; Huang, M.; Tao, H.; Ma, X.; Ni, Z.; Tian, H.; Chen, X. UV Rewritable Hybrid Graphene/Phosphor p–n Junction Photodiode. *ACS Appl. Mater. Interfaces* **2019**, *11* (46), 43351–43358.
- (13) Le, O. K.; Chihaia, V.; Pham-Ho, M.-P.; Son, D. N. Electronic and Optical Properties of Monolayer MoS<sub>2</sub> under the Influence of Polyethyleneimine Adsorption and Pressure. *RSC Adv.* **2020**, *10* (8), 4201–4210.
- (14) Utama, M. I. B.; Kleemann, H.; Zhao, W.; Ong, C. S.; da Jornada, F. H.; Qiu, D. Y.; Cai, H.; Li, H.; Kou, R.; Zhao, S.; Wang, S.; Watanabe, K.; Taniguchi, T.; Tongay, S.; Zettl, A.; Louie, S. G.; Wang, F. A Dielectric-Defined Lateral Heterojunction in a Monolayer Semiconductor. *Nature Electronics* **2019**, *2* (2), 60–65.
- (15) Liu, B.; Zhao, W.; Ding, Z.; Verzhbitskiy, I.; Li, L.; Lu, J.; Chen, J.; Eda, G.; Loh, K. P. Engineering Bandgaps of Monolayer MoS<sub>2</sub> and WS<sub>2</sub> on Fluoropolymer Substrates by Electrostatically Tuned Many-Body Effects. *Advanced Materials* **2016**, *28* (30), 6457–6464.
- (16) Li, Z.; Lv, Y.; Ren, L.; Li, J.; Kong, L.; Zeng, Y.; Tao, Q.; Wu, R.; Ma, H.; Zhao, B.; Wang, D.; Dang, W.; Chen, K.; Liao, L.; Duan, X.; Duan, X.; Liu, Y. Efficient Strain Modulation of 2D Materials *via* Polymer Encapsulation. *Nature Communications* **2020**, *11* (1), 1151.
- (17) O'Malley, K. M.; Li, C.-Z.; Yip, H.-L.; Jen, A. K.-Y. Enhanced Open-Circuit Voltage in High Performance Polymer/Fullerene Bulk-Heterojunction Solar Cells by Cathode Modification with a C<sub>60</sub> Surfactant. *Advanced Energy Materials* **2012**, *2* (1), 82–86.
- (18) Seo, J. H.; Yang, R.; Brzezinski, J. Z.; Walker, B.; Bazan, G. C.; Nguyen, T.-Q. Electronic Properties at Gold/Conjugated-Polyelectrolyte Interfaces. *Advanced Materials* **2009**, *21* (9), 1006–1011.
- (19) Liu, Y.; Duzhko, V. V.; Page, Z. A.; Emrick, T.; Russell, T. P. Conjugated Polymer Zwitterions: Efficient Interlayer Materials in Organic Electronics. *Acc. Chem. Res.* **2016**, *49* (11), 2478–2488.

- (20) Liu, Y.; Page, Z.; Ferdous, S.; Liu, F.; Kim, P.; Emrick, T.; Russell, T. Dual Functional Zwitterionic Fullerene Interlayer for Efficient Inverted Polymer Solar Cells. *Advanced Energy Materials* **2015**, *5* (14), 1500405.
- (21) Liu, Y.; Sheri, M.; Cole, M. D.; Emrick, T.; Russell, T. P. Combining Fullerenes and Zwitterions in Non-Conjugated Polymer Interlayers to Raise Solar Cell Efficiency. *Angewandte Chemie International Edition* **2018**, *57* (31), 9675–9678.
- (22) Duan, C.; Wang, L.; Zhang, K.; Guan, X.; Huang, F. Conjugated Zwitterionic Polyelectrolytes and Their Neutral Precursor as Electron Injection Layer for High-Performance Polymer Light-Emitting Diodes. *Advanced Materials* **2011**, *23* (14), 1665–1669.
- (23) Hoven, C.; Yang, R.; Garcia, A.; Heeger, A. J.; Nguyen, T.-Q.; Bazan, G. C. Ion Motion in Conjugated Polyelectrolyte Electron Transporting Layers. *J. Am. Chem. Soc.* **2007**, *129* (36), 10976–10977.
- (24) Garcia, A.; Bakus II, R. C.; Zalar, P.; Hoven, C. V.; Brzezinski, J. Z.; Nguyen, T.-Q. Controlling Ion Motion in Polymer Light-Emitting Diodes Containing Conjugated Polyelectrolyte Electron Injection Layers. *J. Am. Chem. Soc.* **2011**, *133* (8), 2492–2498.
- (25) Yang, R.; Wu, H.; Cao, Y.; Bazan, G. C. Control of Cationic Conjugated Polymer Performance in Light Emitting Diodes by Choice of Counterion. *J. Am. Chem. Soc.* **2006**, *128* (45), 14422–14423.
- (26) Zakhidov, A. A.; Lee, J.-K.; DeFranco, J. A.; Fong, H. H.; Taylor, P. G.; Chatzichristidi, M.; Ober, C. K.; Malliaras, G. G. Orthogonal Processing: A New Strategy for Organic Electronics. *Chem. Sci.* **2011**, 2 (6), 1178–1182.
- (27) Ruscello, M.; Stolz, S.; Gonzalez Arellano, D. L.; Ullrich, F.; Hillebrandt, S.; Mankel, E.; Pucci, A.; Kowalsky, W.; Emrick, T.; Briseno, A. L.; Hernandez-Sosa, G. Electron Injection and Interfacial Trap Passivation in Solution-Processed Organic Light-Emitting Diodes Using a Polymer Zwitterion Interlayer. *Organic Electronics* **2017**, *50*, 384–388.
- (28) Li, Z.; Chen, Q.; Liu, Y.; Ding, L.; Zhang, K.; Zhu, K.; Yuan, L.; Dong, B.; Zhou, Y.; Song, B. A Nonconjugated Zwitterionic Polymer: Cathode Interfacial Layer Comparable with PFN for Narrow-Bandgap Polymer Solar Cells. *Macromolecular Rapid Communications* **2018**, *39* (14), 1700828.
- (29) Chen, Q.; Yuan, L.; Duan, R.; Huang, P.; Fu, J.; Ma, H.; Wang, X.; Zhou, Y.; Song, B. Zwitterionic Polymer: A Facile Interfacial Material Works at Both Anode and Cathode in *p-i-n* Perovskite Solar Cells. *Solar RRL* **2019**, *3* (9), 1900118.
- (30) Alon, H.; Stern, C.; Kirshner, M.; Sinai, O.; Wasserman, M.; Selhorst, R.; Gasper, R.; Ramasubramaniam, A.; Emrick, T.; Naveh, D. Lithographically Patterned Functional Polymer–Graphene Hybrids for Nanoscale Electronics. *ACS Nano* **2018**, *12* (2), 1928–1933.
- (31) Wang, C.; Luo, Y.; Zheng, J.; Liu, L.; Xie, Z.; Huang, F.; Yang, B.; Ma, Y. Spontaneous Interfacial Dipole Orientation Effect of Acetic Acid Solubilized PFN. *ACS Appl. Mater. Interfaces* **2018**, *10* (12), 10270–10279.
- (32) Chen, L.; Xie, C.; Chen, Y. Self-Assembled Conjugated Polyelectrolyte–Ionic Liquid Crystal Complex as an Interlayer for Polymer Solar Cells: Achieving Performance Enhancement *via* Rapid Liquid Crystal-Induced Dipole Orientation. *Macromolecules* **2014**, *47* (5), 1623–1632.
- (33) Wang, N.; Seymour, B. T.; Lewoczko, E. M.; Kent, E. W.; Chen, M.-L.; Wang, J.-H.; Zhao, B. Zwitterionic Poly(Sulfobetaine Methacrylate)s in Water: From Upper Critical Solution Temperature (UCST) to Lower Critical Solution Temperature (LCST) with Increasing Length of One Alkyl Substituent on the Nitrogen Atom. *Polym. Chem.* **2018**, *9* (43), 5257–5261.
- (34) Chang, C.-C.; Letteri, R.; Hayward, R. C.; Emrick, T. Functional Sulfobetaine Polymers: Synthesis and Salt-Responsive Stabilization of Oil-in-Water Droplets. *Macromolecules* **2015**, *48* (21), 7843–7850.
- (35) Hildebrand, V.; Laschewsky, A.; Päch, M.; Müller-Buschbaum, P.; Papadakis, C. M. Effect of the Zwitterion Structure on the Thermo-Responsive Behaviour of Poly(Sulfobetaine Methacrylates). *Polym. Chem.* **2016**, *8* (1), 310–322.
- (36) Leckey, R. Ultraviolet Photoelectron Spectroscopy of Solids. In *Surface Analysis Methods in Materials Science*; O'Connor, D. J., Sexton, B. A., Smart, R. St. C., Eds.; Springer Series in Surface Sciences; Springer: Berlin, Heidelberg, 2003; pp 337–345.

- (37) Cook, B.; Russakoff, A.; Varga, K. Coverage Dependent Work Function of Graphene on a Cu(111) Substrate with Intercalated Alkali Metals. *Appl. Phys. Lett.* **2015**, *106* (21), 211601.
- (38) Schulzendorf, M.; Hinaut, A.; Kisiel, M.; Jöhr, R.; Pawlak, R.; Restuccia, P.; Meyer, E.; Righi, M. C.; Glatzel, T. Altering the Properties of Graphene on Cu(111) by Intercalation of Potassium Bromide. *ACS Nano* **2019**, *13* (5), 5485–5492.
- (39) Jin, Y.; Kim, H.-U.; Hong, S.; Shin, C.; Kulkarni, A.; Kim, T. Effect of Copper Foil Crystal Orientation on Graphene Quality Synthesized by Chemical Vapor Deposition. *Journal of Nanoscience and Nanotechnology* **2019**, *19* (9), 5942–5948.
- (40) Lee, H.; Puodziukynaite, E.; Zhang, Y.; Stephenson, J. C.; Richter, L. J.; Fischer, D. A.; DeLongchamp, D. M.; Emrick, T.; Briseno, A. L. Poly(Sulfobetaine Methacrylate)s as Electrode Modifiers for Inverted Organic Electronics. *J. Am. Chem. Soc.* **2015**, *137* (1), 540–549.
- (41) Zhou, Z.; Abe, A. A RIS Treatment of the Mean-Square Dipole Moment of PMMA Chains in Consideration of the Pendant Ester Group Orientations. *Polymer* **2004**, *45* (4), 1313–1320.
- (42) Liu, F.; Page, Z. A.; Duzhko, V. V.; Russell, T. P.; Emrick, T. Conjugated Polymeric Zwitterions as Efficient Interlayers in Organic Solar Cells. *Advanced Materials* **2013**, *25* (47), 6868–6873.
- (43) Crispin, X.; Geskin, V.; Crispin, A.; Cornil, J.; Lazzaroni, R.; Salaneck, W. R.; Brédas, J.-L. Characterization of the Interface Dipole at Organic/ Metal Interfaces. *J. Am. Chem. Soc.* **2002**, *124* (27), 8131–8141.
- (44) Zhou, Y.; Fuentes-Hernandez, C.; Shim, J.; Meyer, J.; Giordano, A. J.; Li, H.; Winget, P.; Papadopoulos, T.; Cheun, H.; Kim, J.; Fenoll, M.; Dindar, A.; Haske, W.; Najafabadi, E.; Khan, T. M.; Sojoudi, H.; Barlow, S.; Graham, S.; Brédas, J.-L.; Marder, S. R.; Kahn, A.; Kippelen, B. A Universal Method to Produce Low–Work Function Electrodes for Organic Electronics. *Science* 2012, 336 (6079), 327–332.
- (45) Xia, R.; Leem, D.-S.; Kirchartz, T.; Spencer, S.; Murphy, C.; He, Z.; Wu, H.; Su, S.; Cao, Y.; Kim, J. S.; deMello, J. C.; Bradley, D. D. C.; Nelson, J. Investigation of a Conjugated Polyelectrolyte Interlayer for Inverted Polymer:Fullerene Solar Cells. *Advanced Energy Materials* **2013**, *3* (6), 718–723.
- (46) Koch, N.; Duhm, S.; Rabe, J. P.; Vollmer, A.; Johnson, R. L. Optimized Hole Injection with Strong Electron Acceptors at Organic-Metal Interfaces. *Phys. Rev. Lett.* **2005**, *95* (23), 237601.
- (47) Ishii, H.; Hayashi, N.; Ito, E.; Washizu, Y.; Sugi, K.; Kimura, Y.; Niwano, M.; Ouchi, Y.; Seki, K. Kelvin Probe Study of Band Bending at Organic Semiconductor/Metal Interfaces: Examination of Fermi Level Alignment. *physica status solidi (a)* **2004**, *201* (6), 1075–1094.
- (48) Ishii, H.; Sugiyama, K.; Ito, E.; Seki, K. Energy Level Alignment and Interfacial Electronic Structures at Organic/Metal and Organic/Organic Interfaces. *Advanced Materials* **1999**, *11* (8), 605–625.
- (49) Bagus, P. S.; Staemmler, V.; Wöll, C. Exchangelike Effects for Closed-Shell Adsorbates: Interface Dipole and Work Function. *Phys. Rev. Lett.* **2002**, *89* (9), 096104.
- (50) Witte, G.; Lukas, S.; Bagus, P. S.; Wöll, C. Vacuum Level Alignment at Organic/Metal Junctions: "Cushion" Effect and the Interface Dipole. *Appl. Phys. Lett.* **2005**, *87* (26), 263502.
- (51) Vázquez, H.; Dappe, Y. J.; Ortega, J.; Flores, F. Energy Level Alignment at Metal/Organic Semiconductor Interfaces: "Pillow" Effect, Induced Density of Interface States, and Charge Neutrality Level. *J. Chem. Phys.* **2007**, *126* (14), 144703.
- (52) Khomyakov, P. A.; Giovannetti, G.; Rusu, P. C.; Brocks, G.; van den Brink, J.; Kelly, P. J. First-Principles Study of the Interaction and Charge Transfer between Graphene and Metals. *Phys. Rev. B* **2009**, *79* (19), 195425.
- (53) Porter, G.; Wilkinson, F. Primary Photochemical Processes in Aromatic Molecules. Part 5.—Flash Photolysis of Benzophenone in Solution. *Trans. Faraday Soc.* **1961**, *57* (0), 1686–1691.
- (54) Christensen, S. K.; Chiappelli, M. C.; Hayward, R. C. Gelation of Copolymers with Pendent Benzophenone Photo-Cross-Linkers. *Macromolecules* **2012**, *45* (12), 5237–5246.
- (55) Kresse, G.; Furthmüller, J. Efficient Iterative Schemes for *ab Initio* Total-Energy Calculations Using a Plane-Wave Basis Set. *Phys. Rev. B* **1996**, *54* (16), 11169–11186.

- (56) Kresse, G.; Joubert, D. From Ultrasoft Pseudopotentials to the Projector Augmented-Wave Method. *Phys. Rev. B* **1999**, *59* (3), 1758–1775.
- (57) Blöchl, P. E. Projector Augmented-Wave Method. Phys. Rev. B 1994, 50 (24), 17953–17979.
- (58) Perdew, J. P.; Burke, K.; Ernzerhof, M. Generalized Gradient Approximation Made Simple. *Phys. Rev. Lett.* **1996**, 77 (18), 3865–3868.
- (59) Grimme, S.; Antony, J.; Ehrlich, S.; Krieg, H. A Consistent and Accurate *ab Initio* Parametrization of Density Functional Dispersion Correction (DFT-D) for the 94 Elements H-Pu. *J Chem Phys* **2010**, *132* (15), 154104.
- (60) Lazić, P. CellMatch: Combining Two Unit Cells into a Common Supercell with Minimal Strain. *Computer Physics Communications* **2015**, *197*, 324–334.
- (61) Makov, G.; Payne, M. C. Periodic Boundary Conditions in *ab Initio* Calculations. *Phys. Rev. B* **1995**, 51 (7), 4014–4022.
- (62) Neugebauer, J.; Scheffler, M. Adsorbate-Substrate and Adsorbate-Adsorbate Interactions of Na and K Adlayers on Al(111). *Phys. Rev. B* **1992**, *46* (24), 16067–16080.

## For Table of Contents only



## SUPPORTING INFORMATION

# Electronic Tuning of Monolayer Graphene with Polymeric "Zwitterists"

James Nicolas Pagaduan,<sup>†</sup> Nicholas Hight-Huf,<sup>‡</sup> Avdhoot Datar,<sup>∥</sup> Yehiel Nagar,<sup>⊥</sup> Michael Barnes,<sup>‡</sup> Doron Naveh,<sup>⊥</sup> Ashwin Ramasubramaniam,<sup>\*∥</sup> Reika Katsumata,<sup>\*†</sup> and Todd Emrick<sup>\*†</sup>

<sup>†</sup>Polymer Science and Engineering Department, <sup>‡</sup>Department of Chemistry, and <sup>||</sup>Department of Mechanical and Industrial Engineering, University of Massachusetts, Amherst, MA 01003, USA <sup>|</sup>Faculty of Engineering and Institute for Nanotechnology and Advanced Materials, Bar-Ilan University, Ramat-Gan 52900, Israel

## A. Synthesis of Monomers

**Preparation of ethylmethyl-SBMA (M2)**. The synthesis of [2-(methacryloyloxy)ethyl]ethylmethyl-(3-sulfopropyl)ammonium hydroxide, referred to as ethylmethyl-SBMA, was performed according to **Scheme S1** by modification of a previously reported procedure. <sup>1</sup> 2-(Methylamino)ethanol (5.32 mL, 65.9 mmol) was weighed into a flame-dried 100 mL three-necked round bottom flask equipped with a stir bar. The flask was placed in an oil bath with a preset temperature of 50 °C. 1-Iodoethane (6.42 mL, 79.1 mmol) was added dropwise into the flask from an addition funnel at 50 °C, and the mixture turned yellow and eventually brown. The mixture was stirred at 50 °C for 26 h. After the addition of a solution of NaOH (3.95 g, 98.9 mmol) in H<sub>2</sub>O (10 mL), the mixture became colorless; stirring was continued at 50 °C overnight. The reaction mixture was then transferred to a separatory funnel and extracted with dichloromethane (30 mL) three times. The combined organic phase was washed with saturated aqueous NaCl solution (20 mL) twice, followed by RO (reverse osmosis) water (20 mL) twice. The organic layer was dried over anhydrous MgSO<sub>4</sub> and concentrated by rotary evaporation, affording 2-(ethylmethylamino)ethanol as a colorless liquid (17% yield). <sup>1</sup>H NMR (500 MHz, CDCl<sub>3</sub>): δ/ppm = 3.56 (t, 2H), 3.10 (s, 1H), 2.48 (t, 2H), 2.44 (q, 2H), 2.21 (s, 3H), 1.03 (t, 3H).

**Scheme S1**. Preparation of ethylmethyl-SBMA (emSBMA).

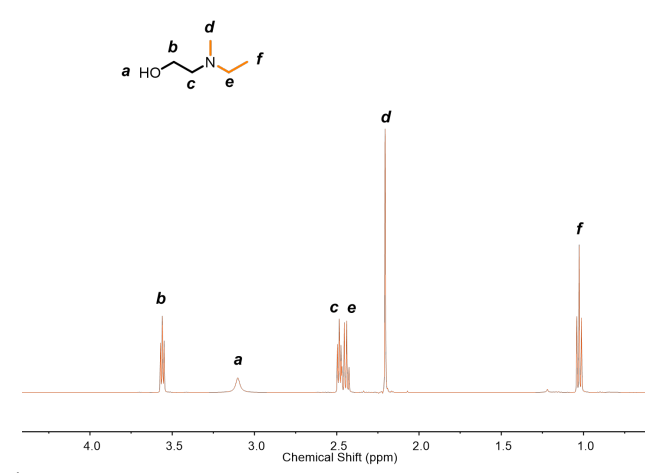


Figure S1. <sup>1</sup>H NMR spectrum of 2-(ethylmethylamino)ethanol (CDCl<sub>3</sub>, 500 MHz).

2-(Ethylmethylamino)ethanol (1.10 g, 10.6 mmol) and triethylamine (2.23 mL, 16.0 mmol) were dissolved in anhydrous dichloromethane (10.6 mL) in a flame-dried 100-mL three-necked flask charged with a stir bar. The mixture was cooled in an ice/water bath for 10 min, and methacryloyl chloride (1.61 mL, 16.0 mmol) was added dropwise from an addition funnel while stirring. The mixture was allowed to warm to room temperature where it was stirred for 24 hours, then transferred to a separatory funnel and washed with saturated NaHCO<sub>3</sub> aqueous solution (50 mL) three times, saturated NaCl aqueous solution (50 mL) twice, and RO water (50 mL) twice. The organic layer was dried over anhydrous MgSO<sub>4</sub> and concentrated by rotary evaporation to afford a yellow liquid, which was purified by column chromatography on silica gel, using ethyl acetate as eluent, to obtain the product in 16% yield. The methacrylate product was dissolved in acetonitrile (0.25 g/mL) with the addition of 1 equivalent of butylated hydroxytoluene (BHT) inhibitor and stored at -80 °C. ¹H NMR (500 MHz, CDCl<sub>3</sub>): δ/ppm = 6.10 (s, 1H), 5.55 (s, 1H), 4.25 (t, 2H), 2.70 (t, 2H), 2.51 (q, 2H), 2.31 (s, 3H), 1.94 (s, 3H), 1.06 (t, 3H).

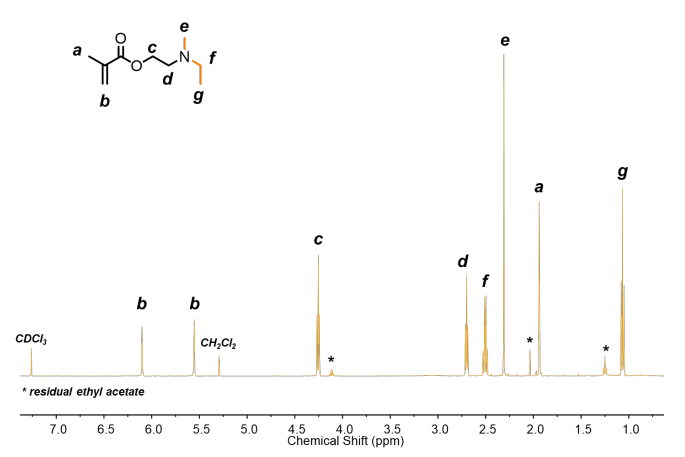


Figure S2. <sup>1</sup>H NMR spectrum of 2-(ethylmethylamino)ethyl methacrylate (CDCl<sub>3</sub>, 500 MHz).

2-(Ethylmethylamino)ethyl methacrylate (0.290 g, 1.69 mmol), 1,3-propanesultone (0.232 g, 1.86 mmol), and BHT (0.377 g, 1.69 mmol) were dissolved in acetonitrile (1.16 mL). The mixture was stirred at 80°C for 48 hours, then cooled to room temperature and concentrated by rotary evaporation. The residue was then dissolved in minimal amount of methanol and precipitated into diethyl ether, then washed several times with diethyl ether to remove any residual BHT, and finally dried under vacuum to afford the product as a white powder (71% yield).  $^{1}$ H NMR (500 MHz,  $D_{2}$ O):  $\delta$ /ppm = 6.16 (s, 1H), 5.79 (s, 1H), 4.63 (t, 2H), 3.80 (t, 2H), 3.54 (m, 4H), 3.15 (s, 3H), 2.98 (t, 2H), 2.24 (m, 2H), 1.95 (s, 3H), 1.39 (t, 3H).

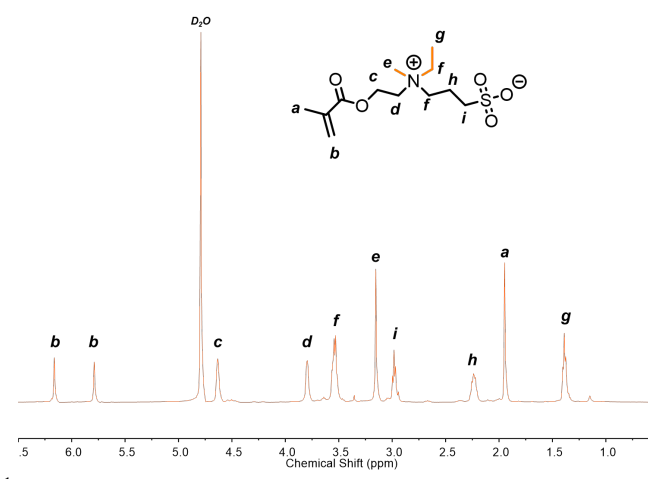


Figure S3. <sup>1</sup>H NMR spectrum of ethylmethyl-SBMA (emSBMA in D<sub>2</sub>O, 500 MHz).

**Preparation of diethyl-SBMA** (M3). [2-(Methacryloyloxy)ethyl]diethyl-(3-sulfopropyl)ammonium hydroxide, referred to as diethyl-SBMA, was prepared according to **Scheme S2** by slight modification of a literature procedure.<sup>2</sup> 1,3-Propanesultone (4.91 g, 39.4 mmol), 2-(diethylamino)ethyl methacrylate (7.26 mL, 35.8 mmol), and 4-methoxyphenol (491 mg, 3.96 mmol) were dissolved in acetonitrile (15 mL). The mixture was stirred at 80°C for 20 hours, then concentrated by rotary evaporation. The residue was then dissolved in a minimal amount of methanol and precipitated into diethyl ether and washed several times with diethyl ether to remove 4-methoxyphenol. Drying of the product under vacuum left the product as a white powder (85% yield). <sup>1</sup>H NMR (500 MHz, D<sub>2</sub>O):  $\delta$ /ppm = 6.17 (s, 1H), 5.81 (s, 1H), 4.62 (t, 2H), 3.76 (t, 2H), 3.49 (m, 6H), 2.99 (t, 2H), 2.22 (m, 2H), 1.96 (s, 3H), 1.37 (t, 6H).

Scheme S2. Preparation of diethyl-SBMA (deSBMA).

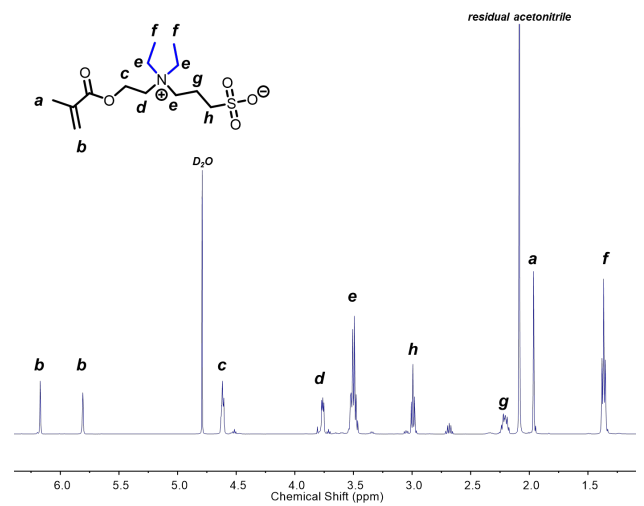


Figure S4. <sup>1</sup>H NMR spectrum of prepared diethyl-SBMA (deSBMA in D<sub>2</sub>O, 500 MHz).

**Preparation of piperidinyl-SBMA (M4).** Piperidinyl-SBMA was synthesized as shown in **Scheme S3** by slight modification of a literature procedure.<sup>3</sup> 2-(Piperidin-1-yl)ethyl methacrylate was first prepared by dissolving 2-piperidinoethanol (5.00 mL, 37.5 mmol) and triethylamine (7.94 mL, 56.9 mmol) in anhydrous dichloromethane (37.9 mL) in a flame-dried 100 mL three-necked flask charged with a stir bar. The mixture was then cooled in an ice/water bath for 10 min, and methacryloyl chloride (5.72 mL, 56.8 mmol) was added dropwise to the stirring reaction mixture by addition funnel. The mixture was allowed to warm to room temperature where it was stirred for 24 hours, then transferred to a separatory funnel and washed with saturated NaHCO<sub>3</sub> aqueous solution (50 mL) three times, saturated NaCl aqueous solution (50 mL) twice, and RO water (50 mL) twice. The organic layer was dried over anhydrous MgSO<sub>4</sub> and concentrated by rotary evaporation to afford the crude product as yellow liquid. Purification by column chromatography on silica gel, eluting with ethyl acetate, gave the product as a colorless liquid (75% yield). <sup>1</sup>H NMR (500 MHz, CDCl<sub>3</sub>):  $\delta$ /ppm = 6.05 (s, 1H), 5.51 (s, 1H), 4.24 (t, 2H), 2.63 (t, 2H), 2.44 (m, 4H), 1.90 (s, 3H), 1.38-1.57 (m, 6H). The product was dissolved in acetonitrile (0.25 g/mL) with the addition of 1 equivalent of butylated hydroxytoluene (BHT) inhibitor and stored at -80 °C.

Scheme S3. Preparation of piperidinyl-SBMA (pipSBMA).

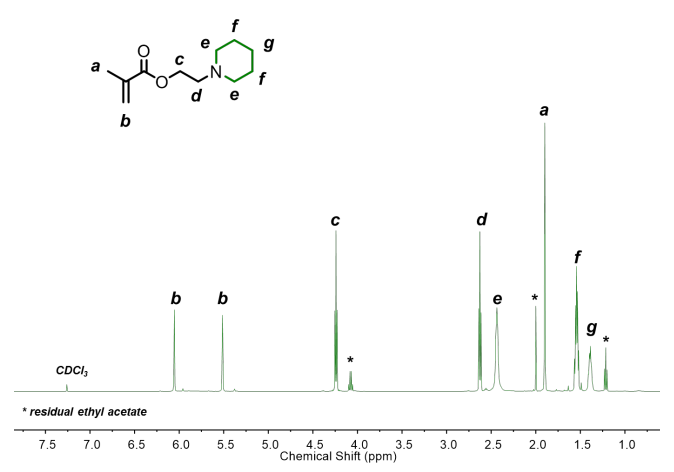


Figure S5. <sup>1</sup>H NMR spectrum of 2-(piperidin-1-yl)ethyl methacrylate (CDCl<sub>3</sub>, 500 MHz).

2-(Piperidin-1-yl)ethyl methacrylate (1.00 g, 5.07 mmol), 1,3-propanesultone (0.688 g, 5.58 mmol), and BHT (1.12 g, 5.07 mmol) were dissolved in acetonitrile (4.0 mL). The mixture was stirred at 80°C for 48 hours, then concentrated by rotary evaporation. The residue was dissolved in minimal amount of methanol and precipitated and washed several times with diethyl ether to remove BHT. Vacuum drying was performed overnight, affording the product as a white powder (36% yield).  $^{1}$ H NMR (500 MHz, D<sub>2</sub>O):  $\delta$ /ppm = 6.15 (s, 1H), 5.79 (s, 1H), 4.63 (t, 2H), 3.85 (t,2H), 3.62 (m, 2H), 3.51 (m, 4H), 2.98 (t, 2H), 2.21 (m, 2H), 1.94 (m, 7H), 1.70 (m, 2H).

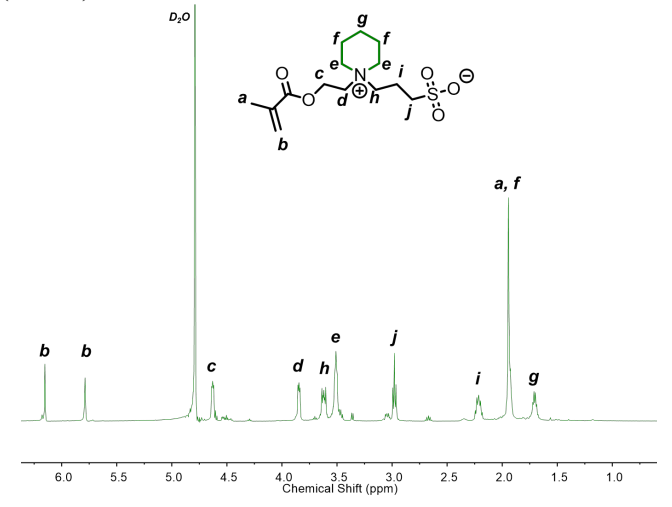


Figure S6. <sup>1</sup>H NMR spectrum of piperidinyl-SBMA (pipSBMA in D<sub>2</sub>O, 500 MHz).

**Preparation of Benzophenone Methacrylamide.** Benzophenone methacrylamide (BPMA) was prepared according to **Scheme S4** based on a previously reported procedure with modifications.<sup>4</sup> 4-Aminobenzophenone (1.00 g, 4.98 mmol) and methacryloyl chloride (0.520 mL, 5.16 mmol) were dissolved in anhydrous dichloromethane (10.0 mL) in a 20 mL scintillation vial equipped with a stir bar and rubber septum. The mixture was cooled in an ice/water bath and triethylamine (0.85 mL, 6.10 mmol) was added slowly. The mixture was allowed to warm to room temperature, then covered with aluminum foil and stirred for 24 hours. The reaction mixture was transferred to a separatory funnel and washed with 1 M HCl, saturated NaHCO<sub>3</sub> solution, and RO water (three times each). The organic phase was dried over anhydrous sodium sulfate and concentrated by rotary evaporation. Vacuum drying was performed

overnight, affording the product as orange solid (64% yield).  $^{1}H$  NMR (500 MHz, CDCl<sub>3</sub>):  $\delta/ppm = 7.45-7.87$  (m, 9H), 7.71 (s, 1H), 5.83 (s, 1H), 5.52 (s, 1H), 2.08 (s, 3H).

Scheme S4. Preparation of benzophenone methacrylamide (BPMA).

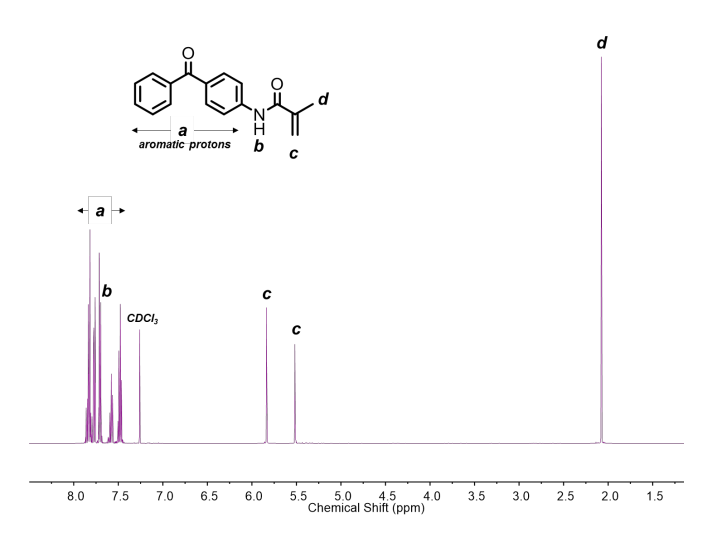


Figure S7. <sup>1</sup>H NMR spectrum of benzophenone methacrylamide (BPMA in CDCl<sub>3</sub>, 500 MHz).

# **B.** Polymer Characterization

**Table S1**. Characterization data for P(xSBMA-MMA-BPMA) copolymers and control samples.

Polymer	Feed Ratio [xSBMA]:[N	Actual Ratio <sup>a</sup> IMA]:[BPMA]	Monomer Conversion (%) <sup>a</sup>	M <sub>n</sub> <sup>b</sup> (kDa)	PDI <sup>b</sup>
P(SBMA-MMA-BPMA)	50:47:3	47:51:2	98	21.3	1.10
P(emSBMA-MMA-BPMA)	50:47:3	48:49:3	98	24.2	1.27
P(deSBMA-MMA-BPMA)	50:47:3	50:48:2	92	28.8	1.20
P(pipSBMA-MMA-BPMA)	50:47:3	49:48:3	90	23.8	1.29
P(MMA-BPMA)	0:97:3	0:98:2	94	20.3	1.09
PMMA	0:100:0	0:100:0	>99	25.5	1.05

a) Determined by <sup>1</sup>H NMR spectroscopy; b) Estimated by GPC relative to PMMA standards, eluting in TFE

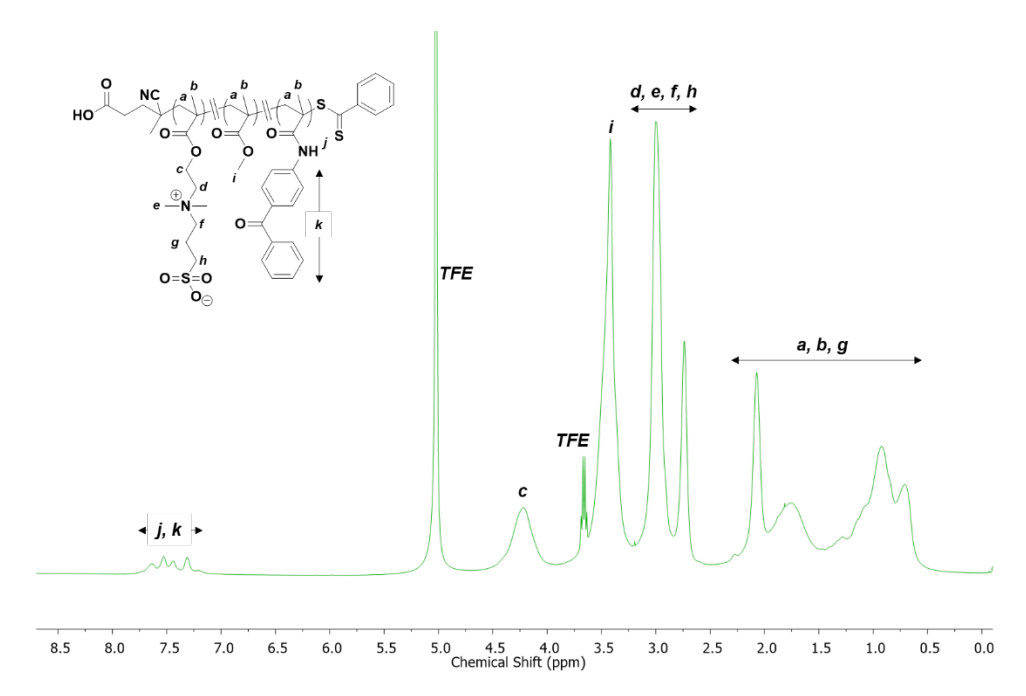
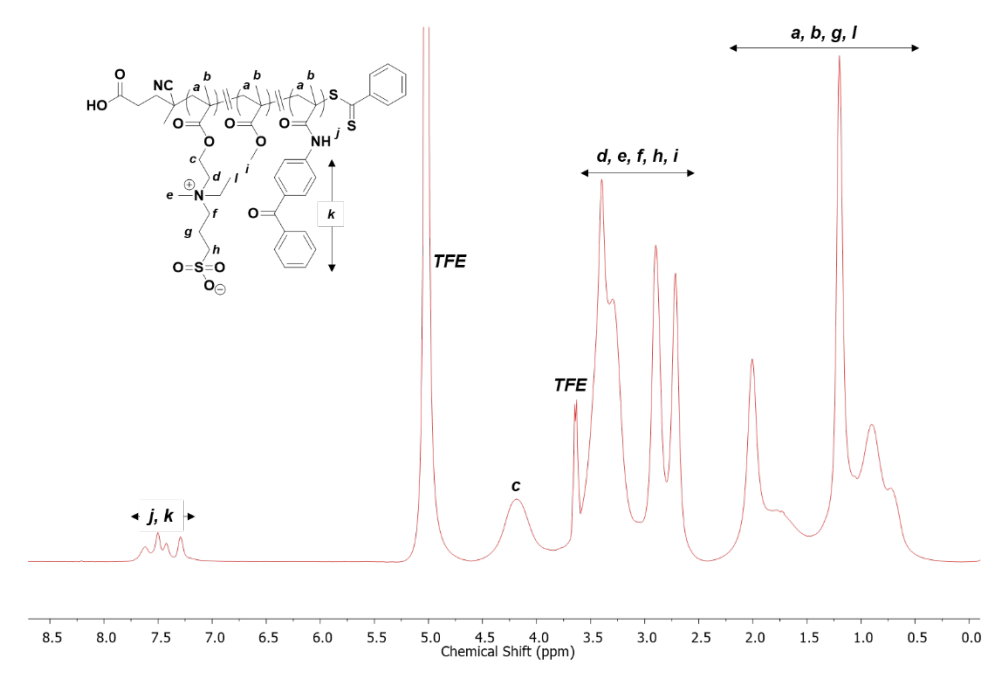


Figure S8. <sup>1</sup>H NMR spectrum of PSBMA copolymer (TFE-d<sub>3</sub>, 500 MHz).



**Figure S9**. <sup>1</sup>H NMR spectrum of PemSBMA copolymer (TFE-d<sub>3</sub>, 500 MHz).

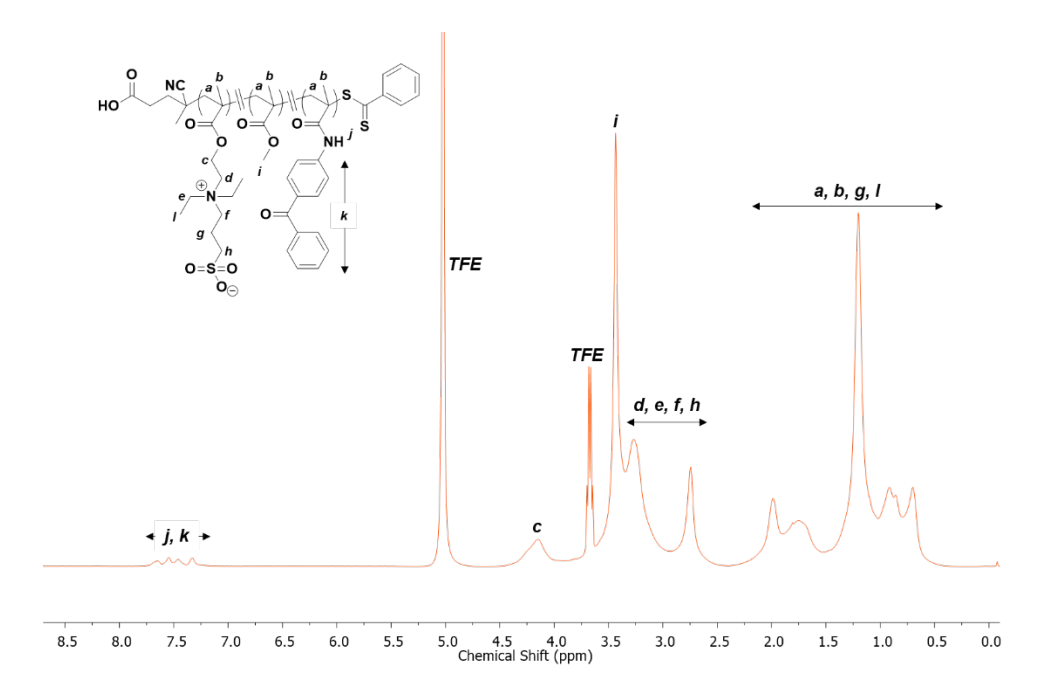
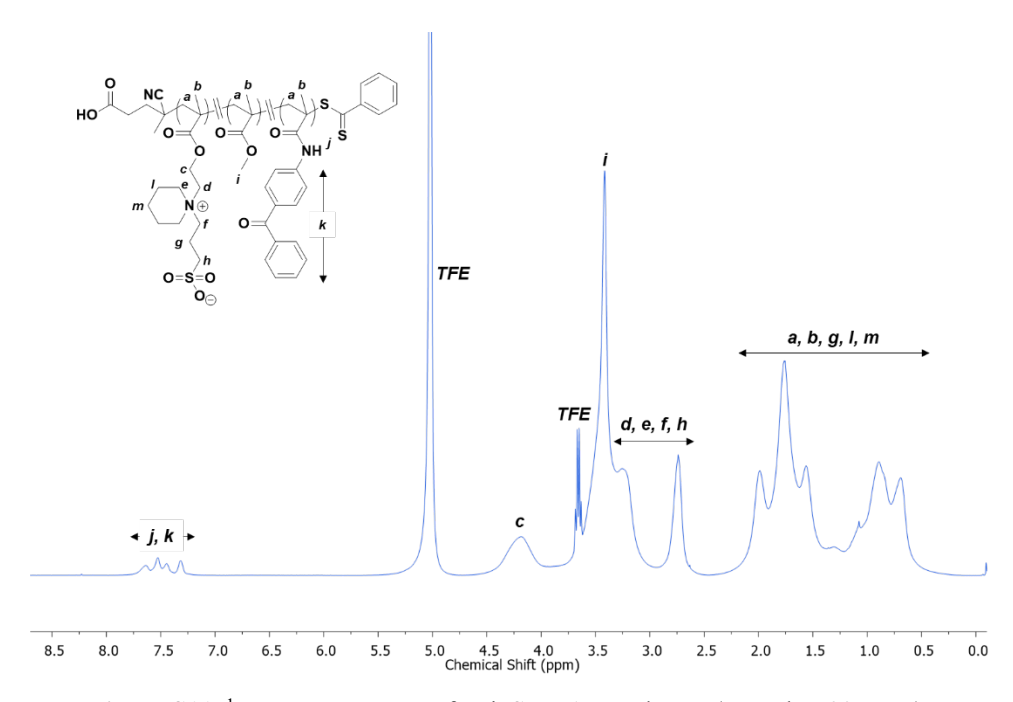
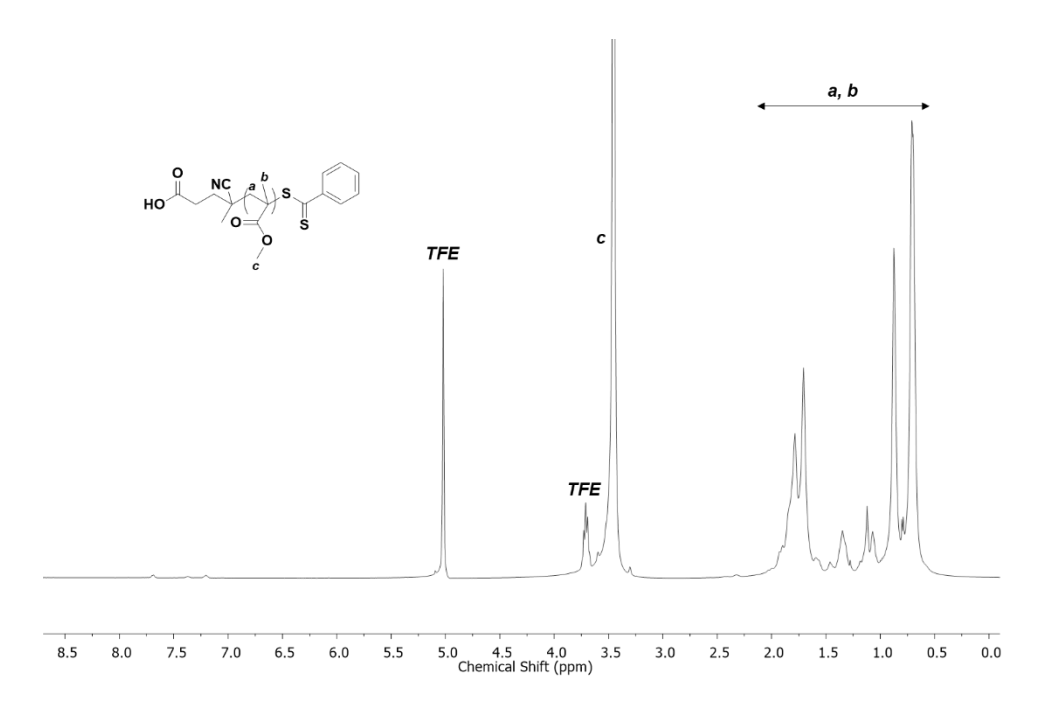


Figure S10. <sup>1</sup>H NMR spectrum of PdeSBMA copolymer (TFE-d<sub>3</sub>, 500 MHz).



**Figure S11**. <sup>1</sup>H NMR spectrum of PpipSBMA copolymer (TFE-d<sub>3</sub>, 500 MHz).



**Figure S12**. <sup>1</sup>H NMR spectrum of PMMA homopolymer (TFE-d3, 500 MHz).

# C. Polymer Film Thickness Measurement

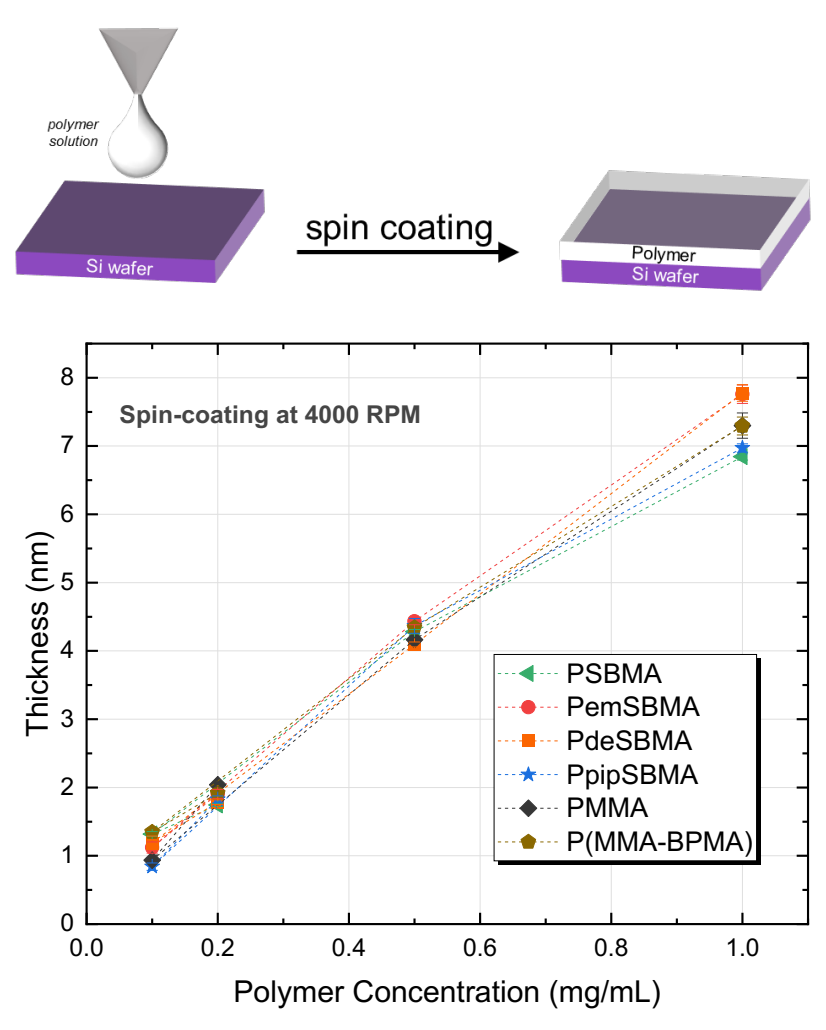


**Figure S13**. Ellipsometry of polymer coatings: preparation of samples (top) and thickness comparison for films obtained from polymer zwitterions and control polymer samples at varying polymer concentrations (bottom).

# D. Ultraviolet Photoelectron Spectroscopy

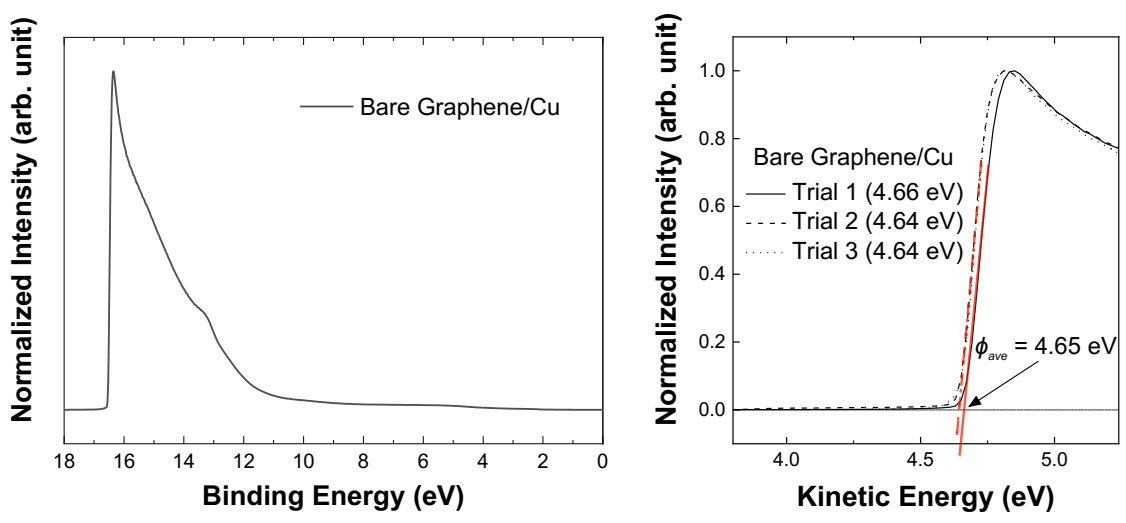


**Figure S14**. Representative full UPS spectrum of bare graphene/Cu (left) and linear fitting of the onset of the secondary electron cut-off (SEC) region for work function determination (right). The reported work function values are averages of at least 3 measurements with 2 different samples.

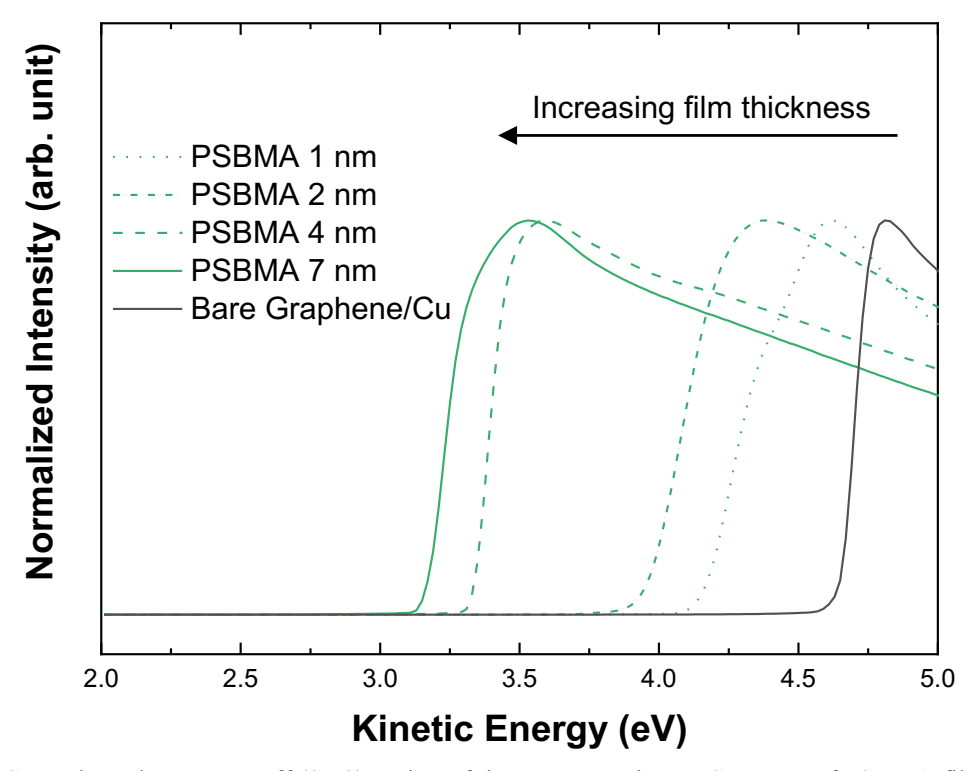


**Figure S15**. Secondary electron cut-off (SEC) region of the representative UPS spectra of PSBMA films of varying thicknesses on graphene/Cu substrate. The nominal thickness values are based on ellipsometry.

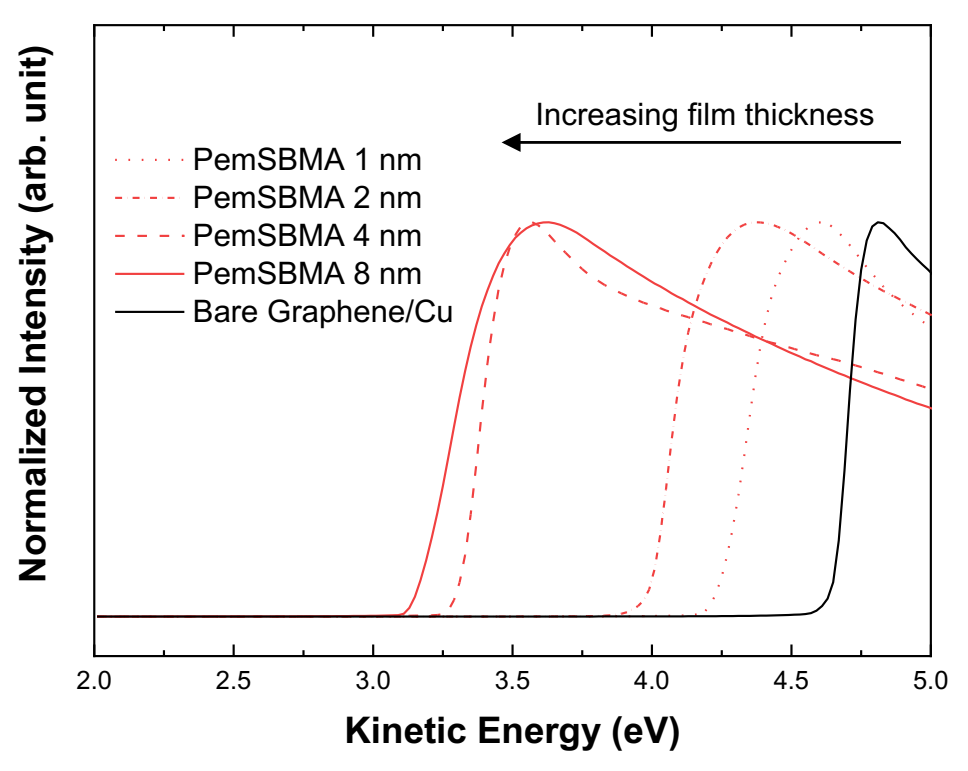


**Figure S16**. SEC region of the representative UPS spectra of PemSBMA films of varying thicknesses on graphene/Cu substrate. The nominal thickness values are based on ellipsometry.

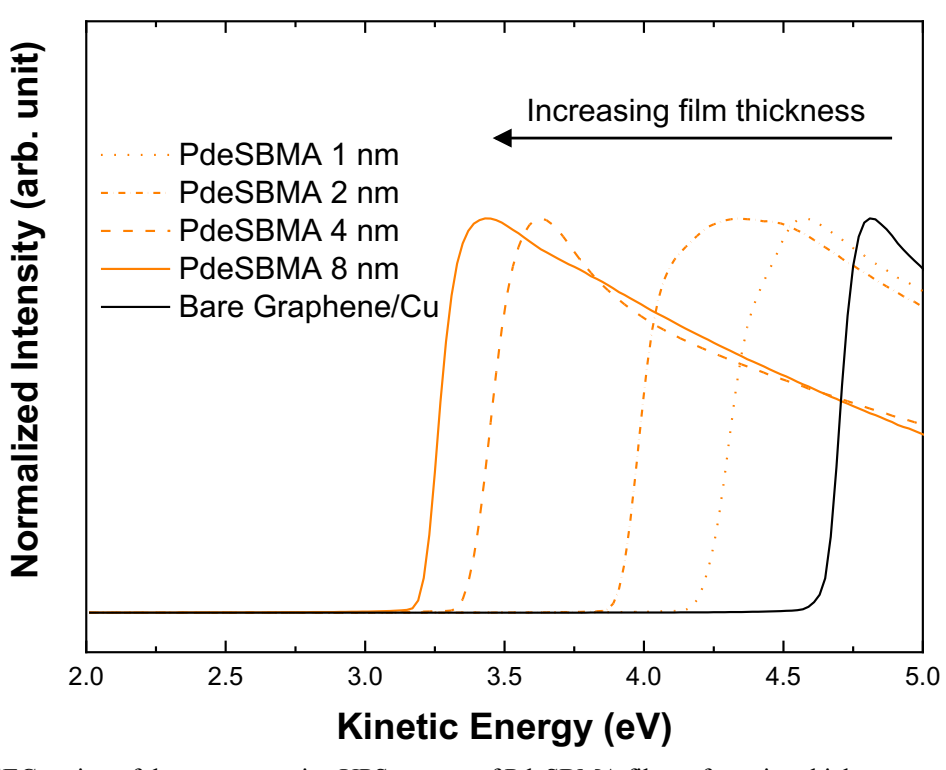


**Figure S17**. SEC region of the representative UPS spectra of PdeSBMA films of varying thicknesses on graphene/Cu substrate. The nominal thickness values are based on ellipsometry.

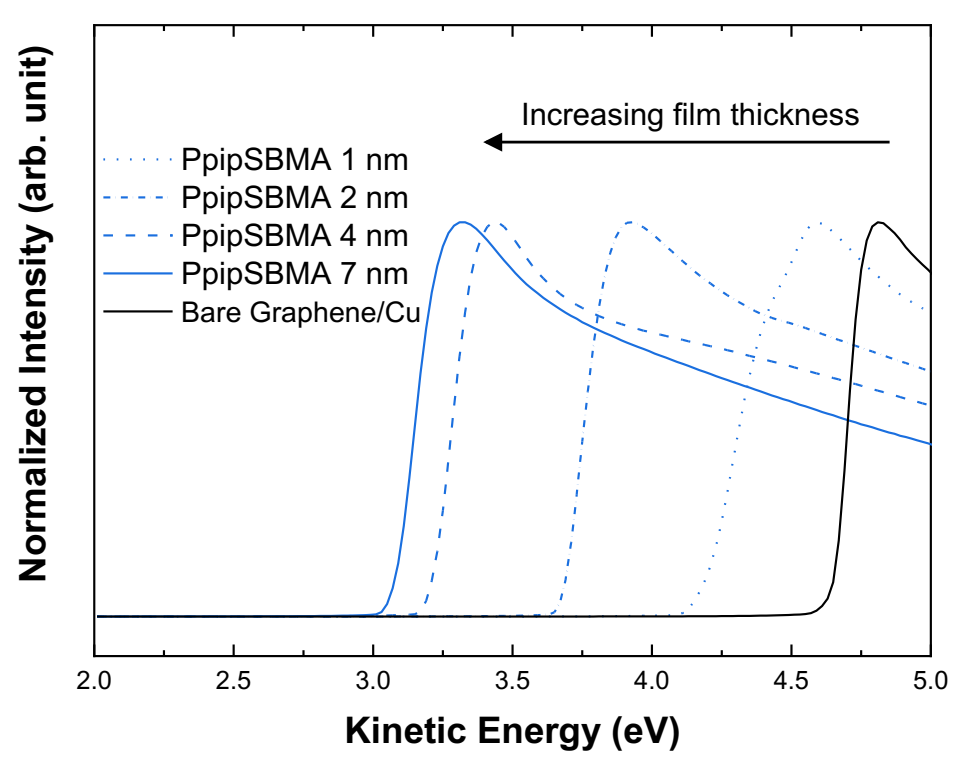


**Figure S18**. SEC region of the representative UPS spectra of PpipSBMA films of varying thicknesses on graphene/Cu substrate. The nominal thickness values are based on ellipsometry.

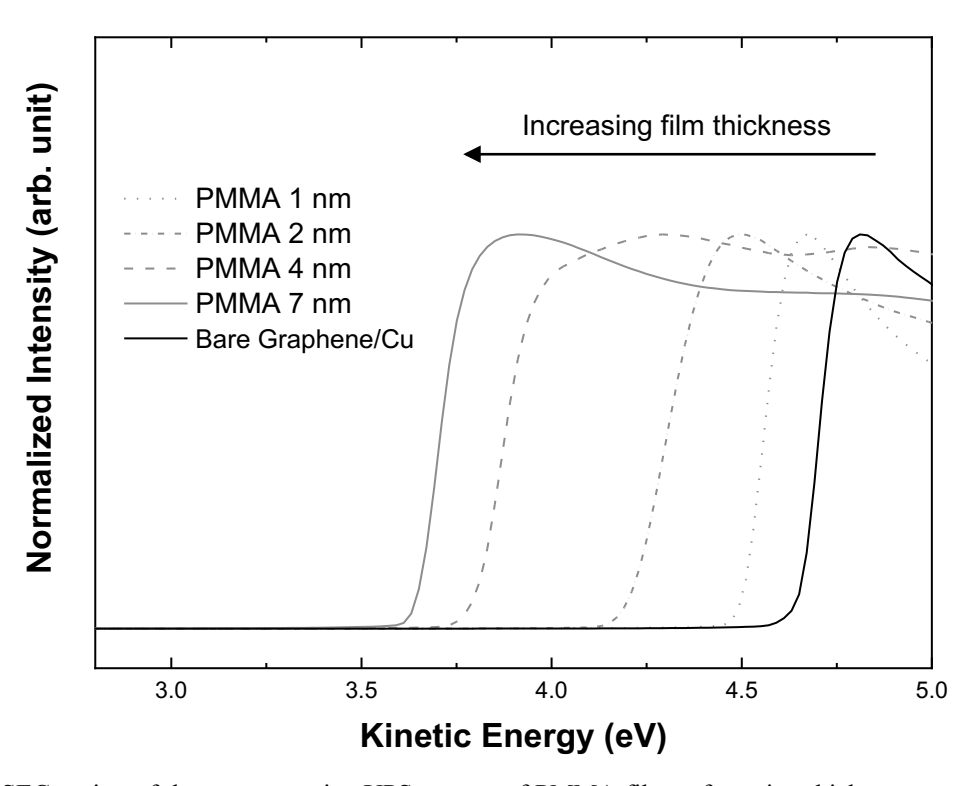


**Figure S19**. SEC region of the representative UPS spectra of PMMA films of varying thicknesses on graphene/Cu substrate. The nominal thickness values are based on ellipsometry.

E. Atomic Force Microscopy of Zwitterionic Polymer Films 85.0 deg PpipSBMA 1 nm PpipSBMA 1 nm RMS = 1 nm80.0 12.0 10.0 75.0 8.0 70.0 6.0 65.0 4.0 60.0 55.0 0.0 20.0 nm 85.0 deg PpipSBMA 2 nm PpipSBMA 2 nm 18.0 RMS = 2 nm80.0 16.0 14.0 75.0 12.0 10.0 70.0 8.0 65.0 6.0 4.0 60.0 0.0 20.0 nm 85.0 deg PpipSBMA 4 nm PpipSBMA 4 nm 18.0 80.0 RMS = 2 nm 16.0 75.0 14.0 70.0 12.0 10.0 65.0 8.0 60.0 6.0 55.0 4.0 0.0 45.0 25.0 nm 85.0 deg PpipSBMA 8 nm PpipSBMA 8 nm 80.0 RMS = 2 nm 20.0 75.0 70.0 15.0 65.0 10.0 60.0 55.0 5.0 3 µm 0.0 45.0 15.0 nm 85.0 deg **Bare Graphene** Bare Graphene 80.0 RMS = 2 nm12.0 75.0 10.0

Figure S20. AFM height (left) and phase (right) images of PpipSBMA films of varying thicknesses on graphene supported on a Si/SiO<sub>2</sub> substrate. The nominal thickness values are based on ellipsometry.

8.0

6.0

70.0

65.0

60.0

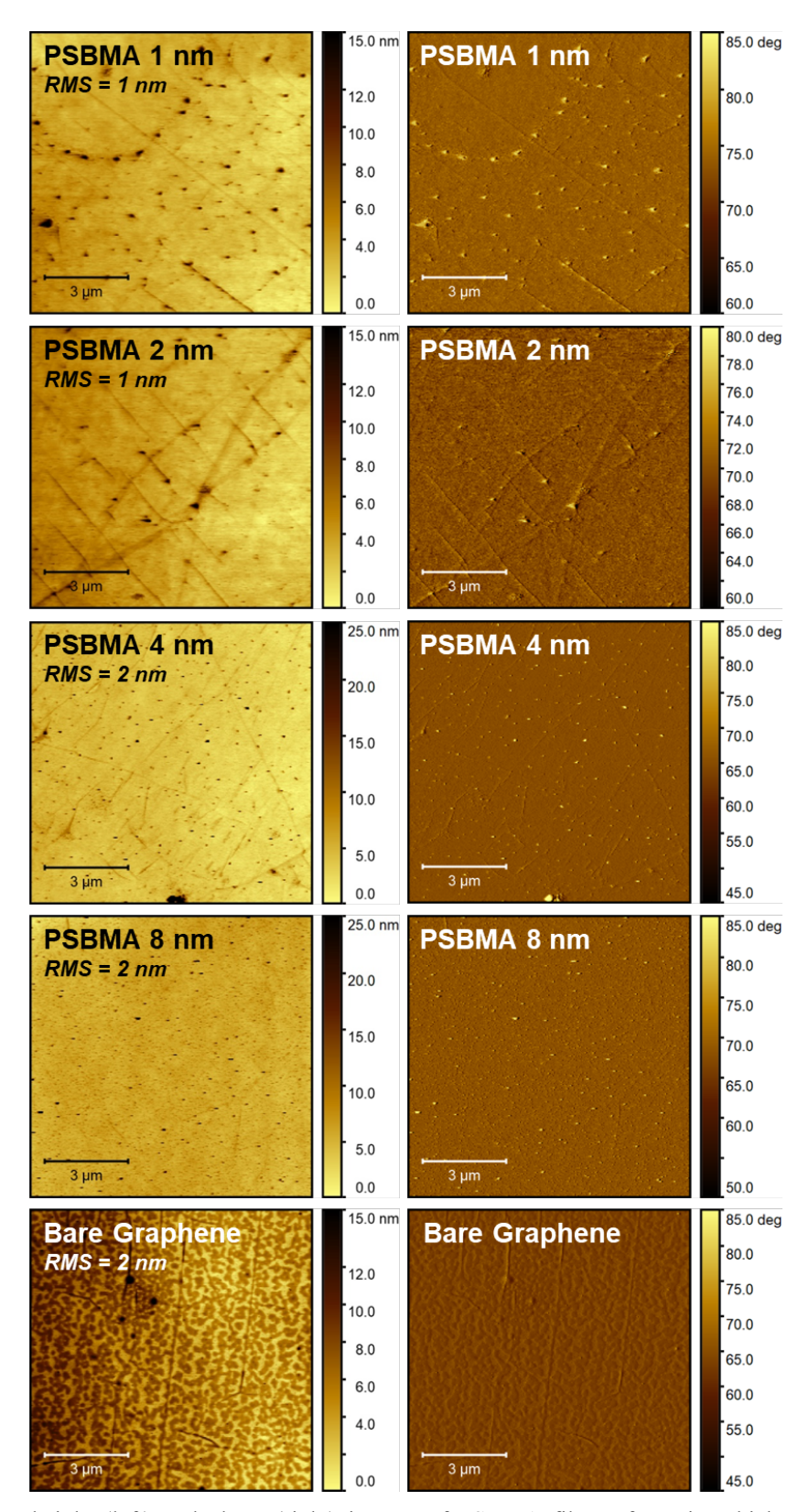
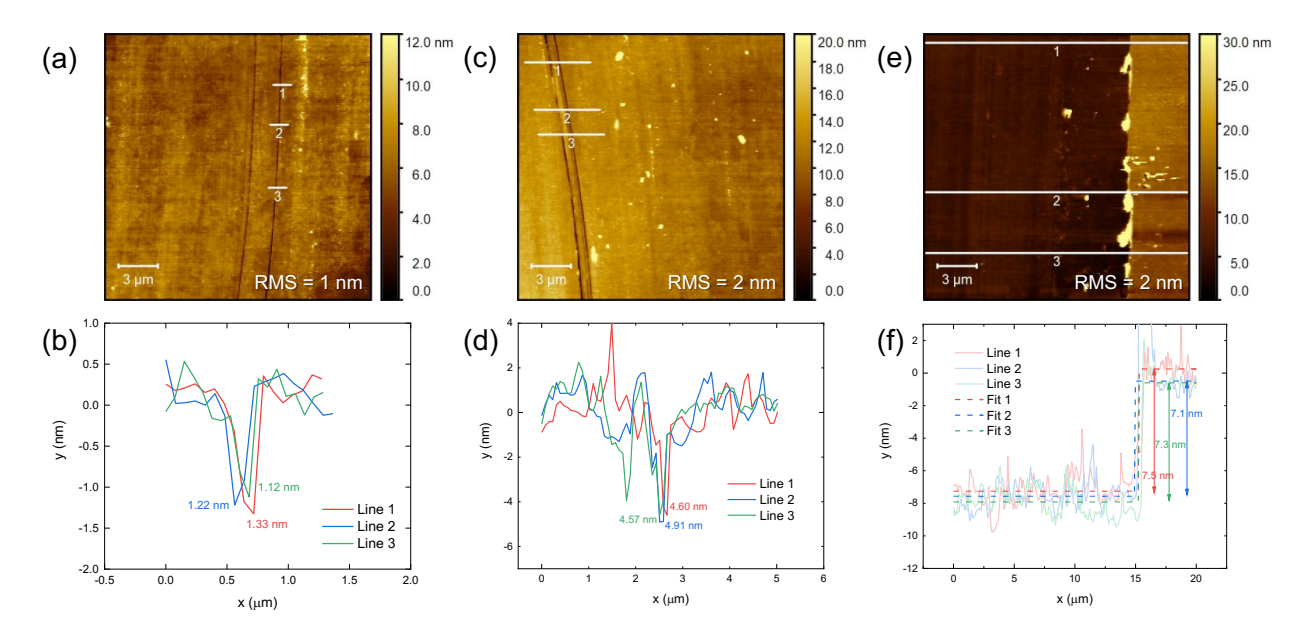
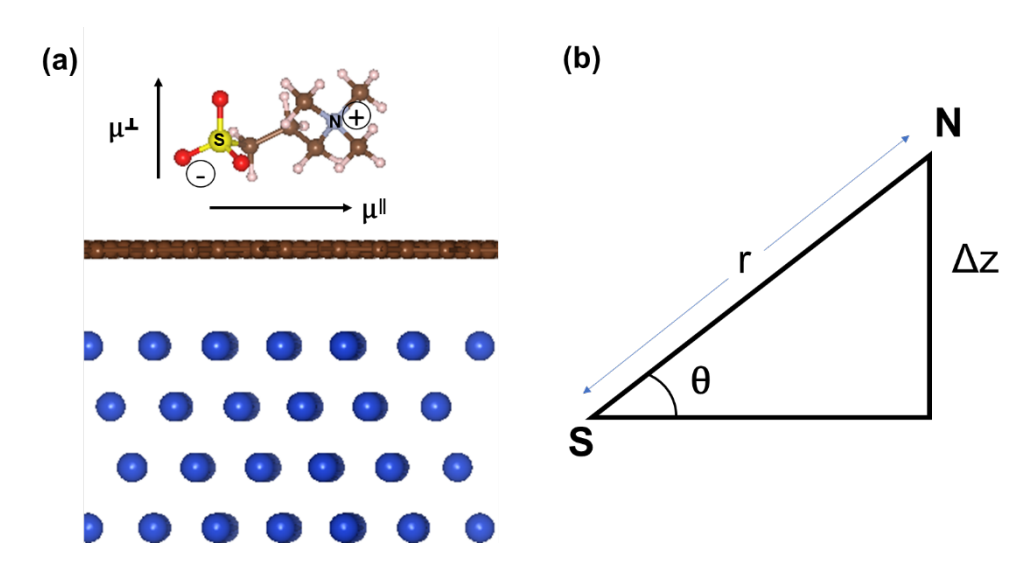


Figure S21. AFM height (left) and phase (right) images of PSBMA films of varying thicknesses on graphene supported on a  $Si/SiO_2$  substrate. The nominal thickness values are based on ellipsometry.



**Figure S22.** AFM height images (top) and step height profiles (bottom) of PpipSBMA films of varying thicknesses (a,b) 1 nm, (c,d) 4 nm and (e,f) 7 nm (nominal thickness based on ellipsometry) on graphene supported on a Si/SiO<sub>2</sub> substrate. Graphene was exposed by scratching the polymer films with a clean 18G needle.

## F. Supplementary DFT Calculations



**Figure S23**. (a) Perpendicular and parallel components of dipole moment. (b) Definition of dipole orientation or tilt angle  $\theta$ . The calculated  $\theta$  values are 8.4°, 2.18°, 0.45°, and 15.8° for SBMA, emSBMA, deSBMA, and pipSBMA, respectively.

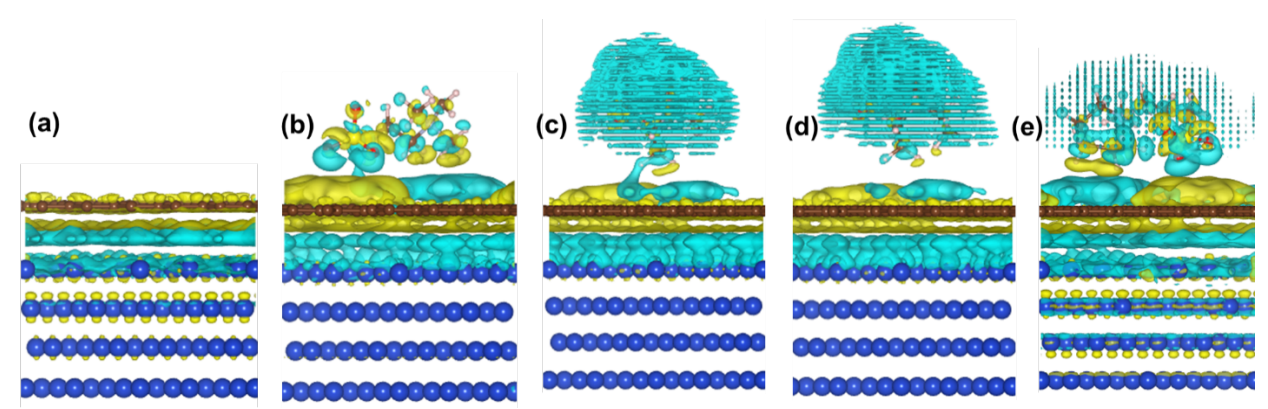


**Figure S24**. Charge-transfer plots for SBMA and its derivatives interacting with graphene (Gr; brown)/Cu (blue) slab; yellow and cyan isosurfaces  $(2 \times 10^{-4} \text{ e/Å}^3)$  indicate charge accumulation and depletion, respectively for (a) Gr/Cu slab, (b) SBMA on Gr/Cu, (c) emSBMA on Gr/Cu, (d) deSBMA on Gr/Cu, and (e) pipSBMA on Gr/Cu.

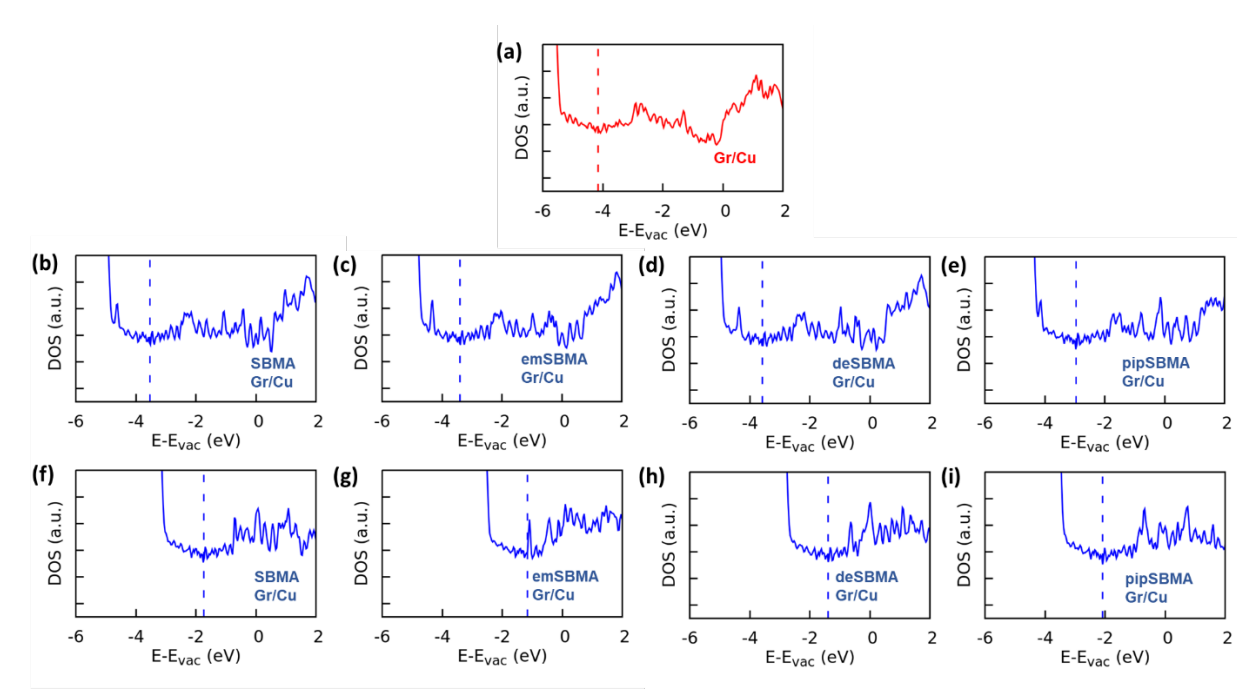


**Figure S25**. Density of states (DOS) plots for (a) Gr/Cu slab, horizontally oriented or flat (b) SBMA, (c) emSBMA, (d) deSBMA, (e) pipSBMA on Gr/Cu slabs, and vertically oriented or standing (f) SBMA, (g) emSBMA, (h) deSBMA, (i) pipSBMA on Gr/Cu slabs. Dotted line in each plot represents placement of Fermi energy.

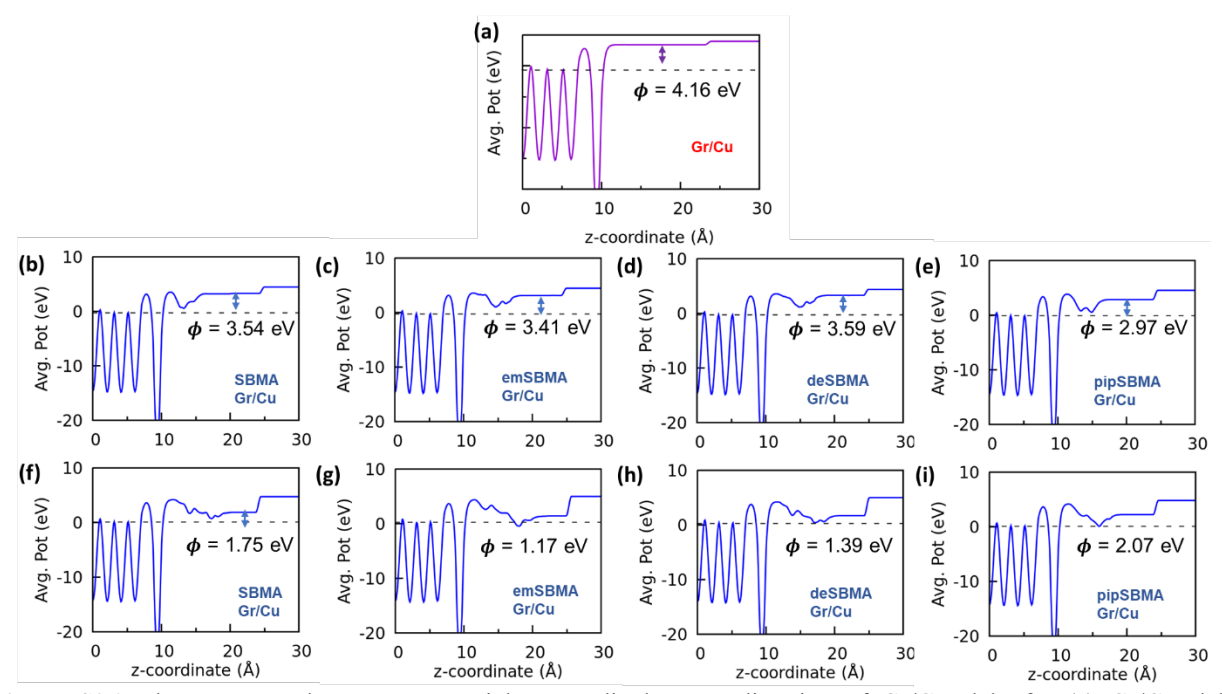


**Figure S26**. Planar-averaged Hartree potential perpendicular to z-direction of Gr/Cu slab, for (a) Gr/Cu slab, horizontally oriented or flat (b) SBMA, (c) emSBMA, (d) deSBMA, (e) pipSBMA on Gr/Cu slabs, and vertically oriented or standing (f) SBMA, (g) emSBMA, (h) deSBMA, (i) pipSBMA on Gr/Cu slabs. Dotted line in each plot represents placement of the Fermi energy. Work functions of pendent adsorbed side for each slab are given in the plot.

**Table S2**. Relative energies  $\Delta E$  of vertically oriented pendent molecule on Gr sheet with respect to horizontally oriented pendent on Gr sheet. Perpendicular component of dipole moment  $(\mu^{\perp})$ . Change in work function  $(\Delta \phi)$  due to pendent molecule with respect to work function of bare Gr sheet  $(\phi = 4.24 \text{ eV})$ .

Pendent	Δ <i>E</i> (eV)	Flat Configuration		Standing Configuration		
Structure		μ <sup>1</sup> (D)	<b>ΔΦ</b> (eV)	μ <sup>1</sup> (D)	<b>ΔΦ</b> (eV)	
SBMA	0.13	1.80	0.36	10.09	2.23	
emSBMA	1.27	2.24	0.46	17.21	3.25	
deSBMA	0.11	2.14	0.44	9.39	1.88	
pipSBMA	0.60	5.19	1.04	12.52	2.51	

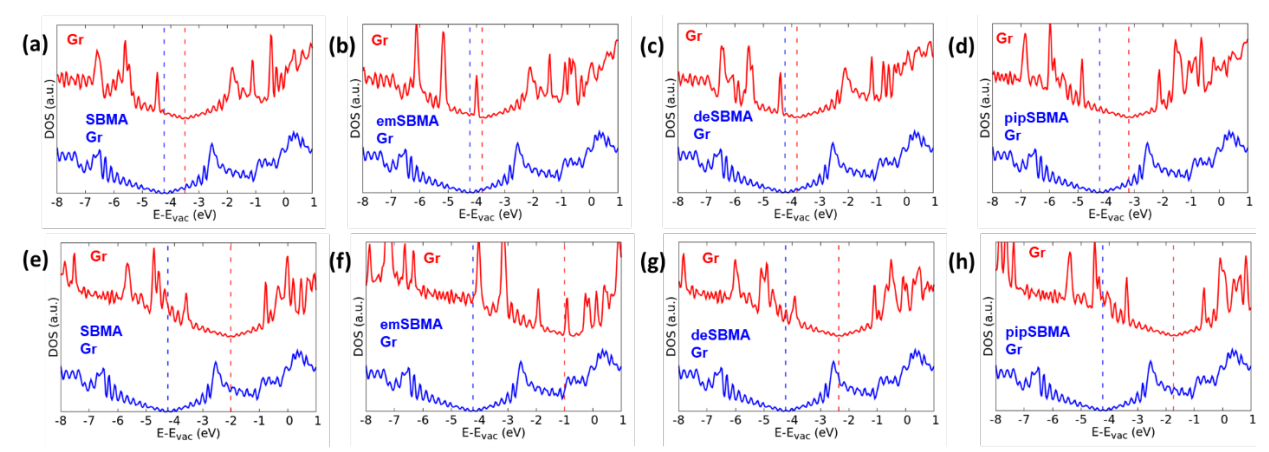


**Figure S27**. DOS plots for horizontally oriented or flat (a) SBMA, (b) emSBMA, (c) deSBMA, (d) pipSBMA on freestanding Gr monolayer, and vertically oriented or standing (e) SBMA, (f) emSBMA, (g) deSBMA, (h) pipSBMA on Gr sheet. Dotted line in each plot represents placement of Fermi energy.

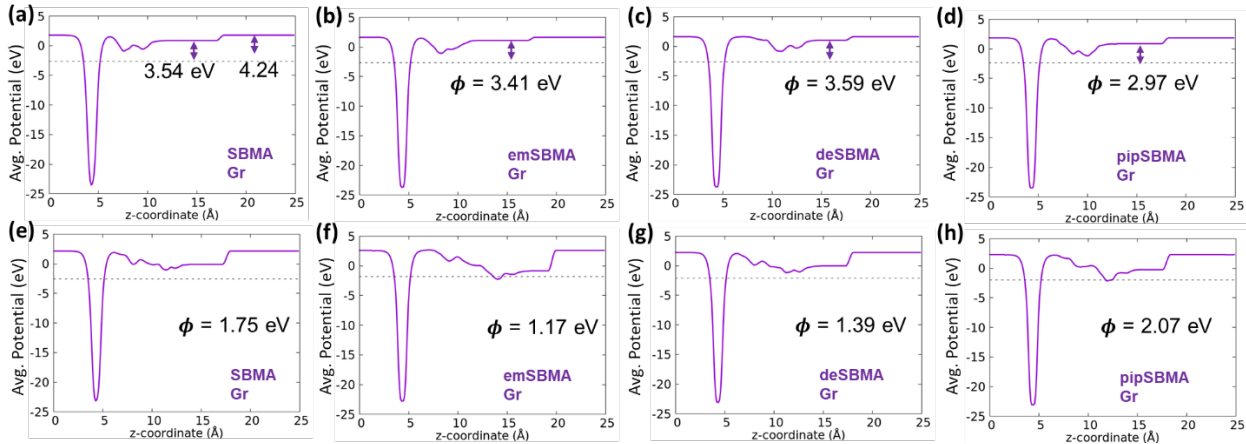


**Figure S28**. Planar-averaged Hartree potential perpendicular to z-direction of freestanding Gr monolayer, for horizontally oriented or flat (a) SBMA, (b) emSBMA, (c) deSBMA, (d) pipSBMA on Gr sheet, and vertically oriented or standing (e) SBMA, (f) emSBMA, (g) deSBMA, (h) pipSBMA on Gr sheet. Dotted line in each plot represents placement of the Fermi energy. Work functions of pendent adsorbed side for each slab are given in the plot.

# G. Optical Microscopy of Zwitterist Before and After UV Lithography

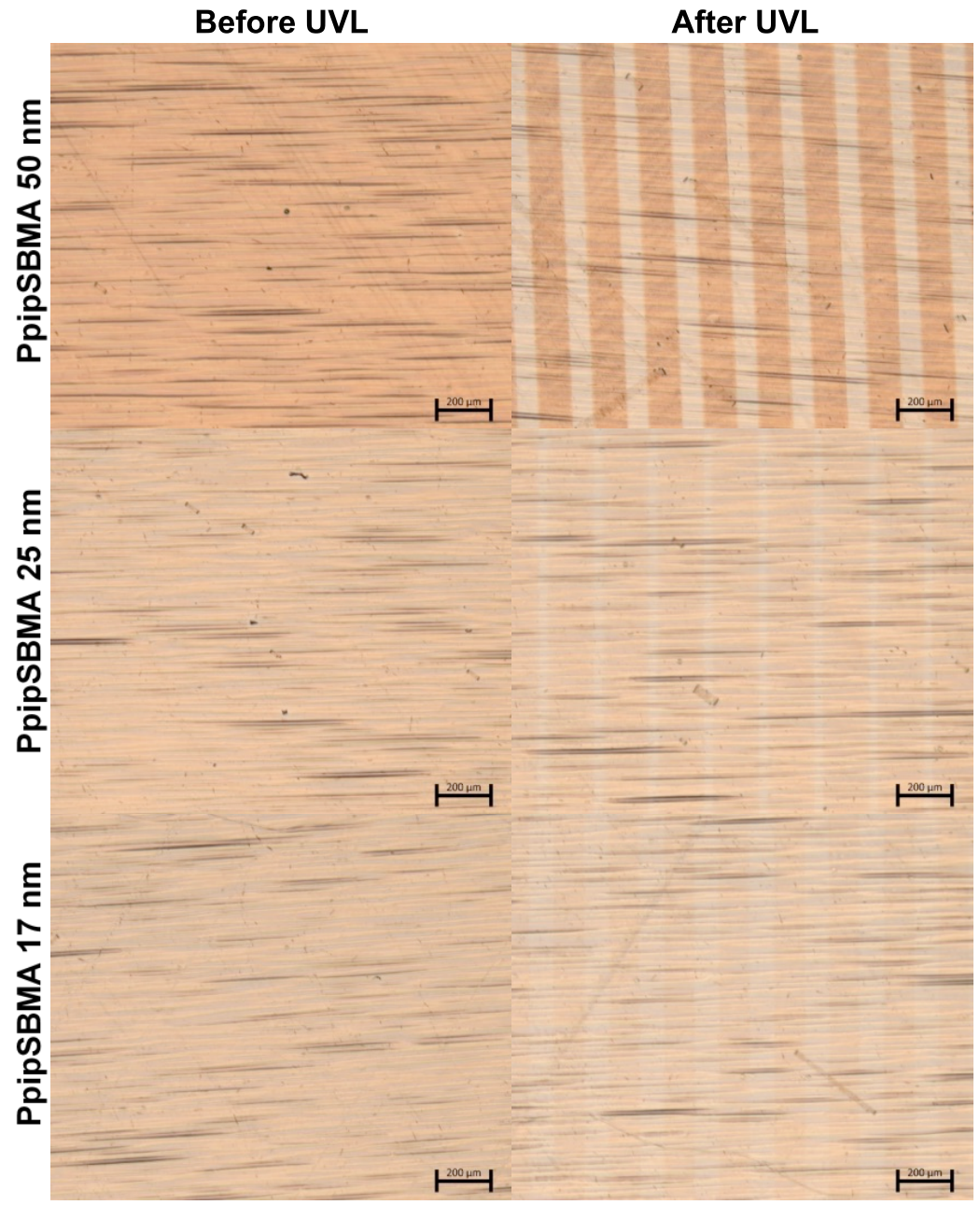


**Figure S29**. Optical micrographs of PpipSBMA films of varying thicknesses on graphene/Cu substrate before and after UV lithography through a photomask. The thicknesses correspond to values estimated from ellipsometry of polymer coatings before UV lithography. The horizontal lines are from graphene/copper surface topography.

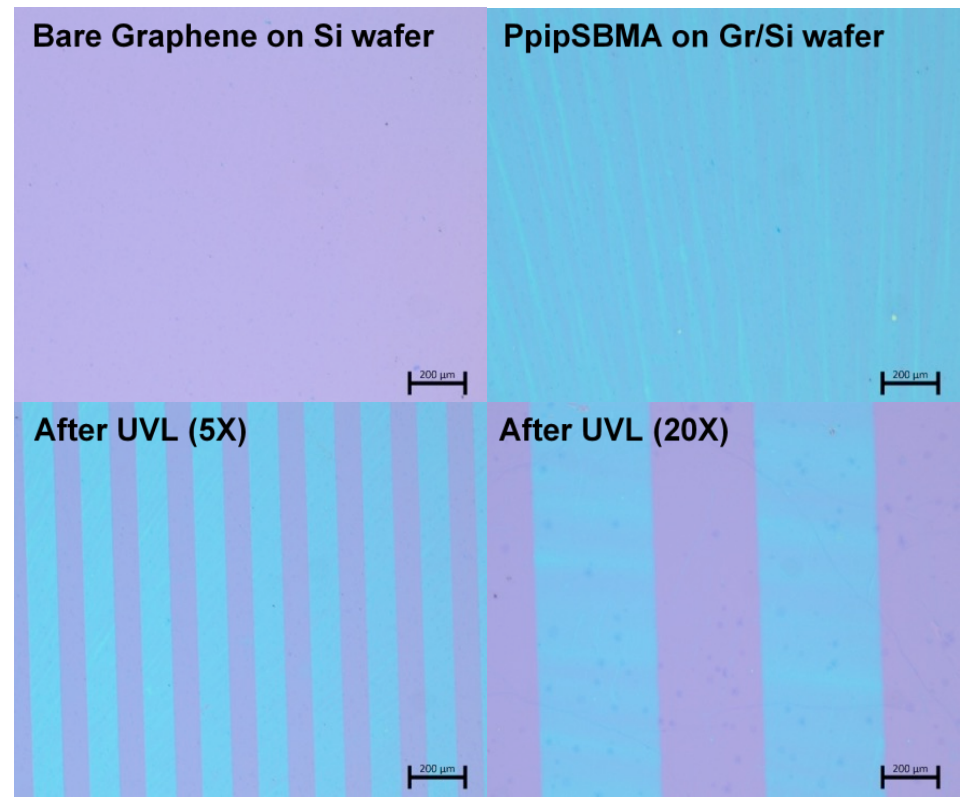


**Figure S30**. Optical micrographs of PpipSBMA film (with an estimated thickness of 25 nm before UV lithography) patterned on graphene supported on a Si/SiO<sub>2</sub> substrate.

# H. Kelvin Probe Force Microscopy of Unpatterned Polymer Films

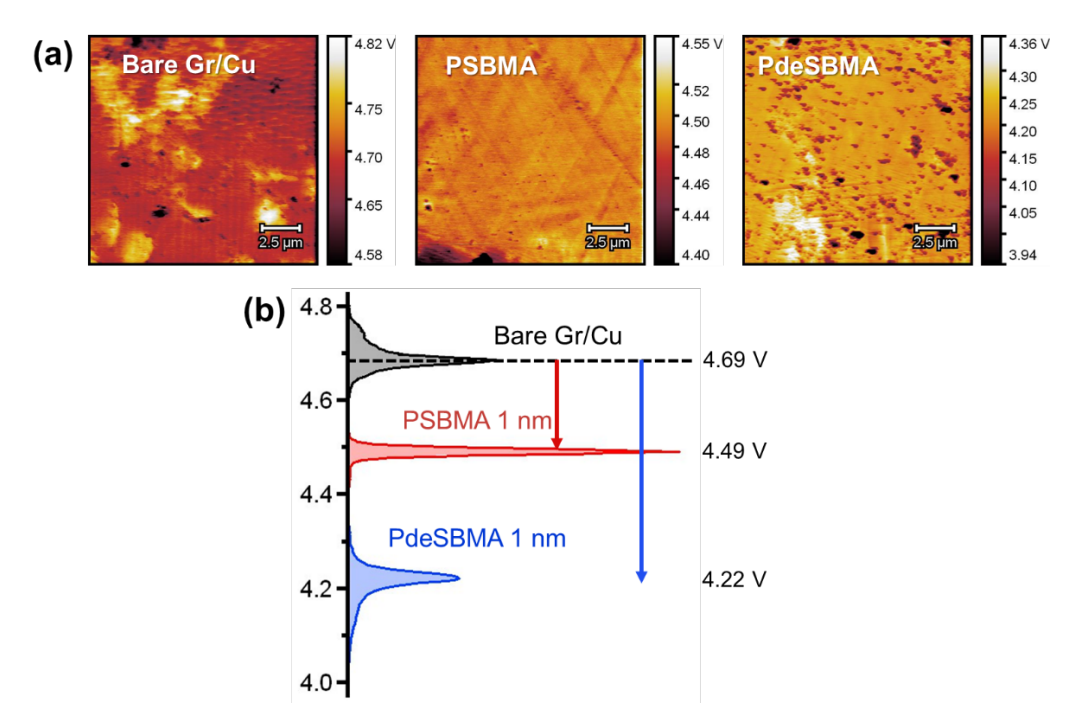


**Figure S31**. (a) Surface potential contrast (SPC) profiles of bare graphene/Cu and graphene/Cu coated with unpatterned PSBMA and PdeSBMA, and (b) normalized SPC distributions of bare and polymer-coated samples, indicating the shift in work function.

## I. Electrical Transport Measurements on Fabricated Graphene Field Effect Devices

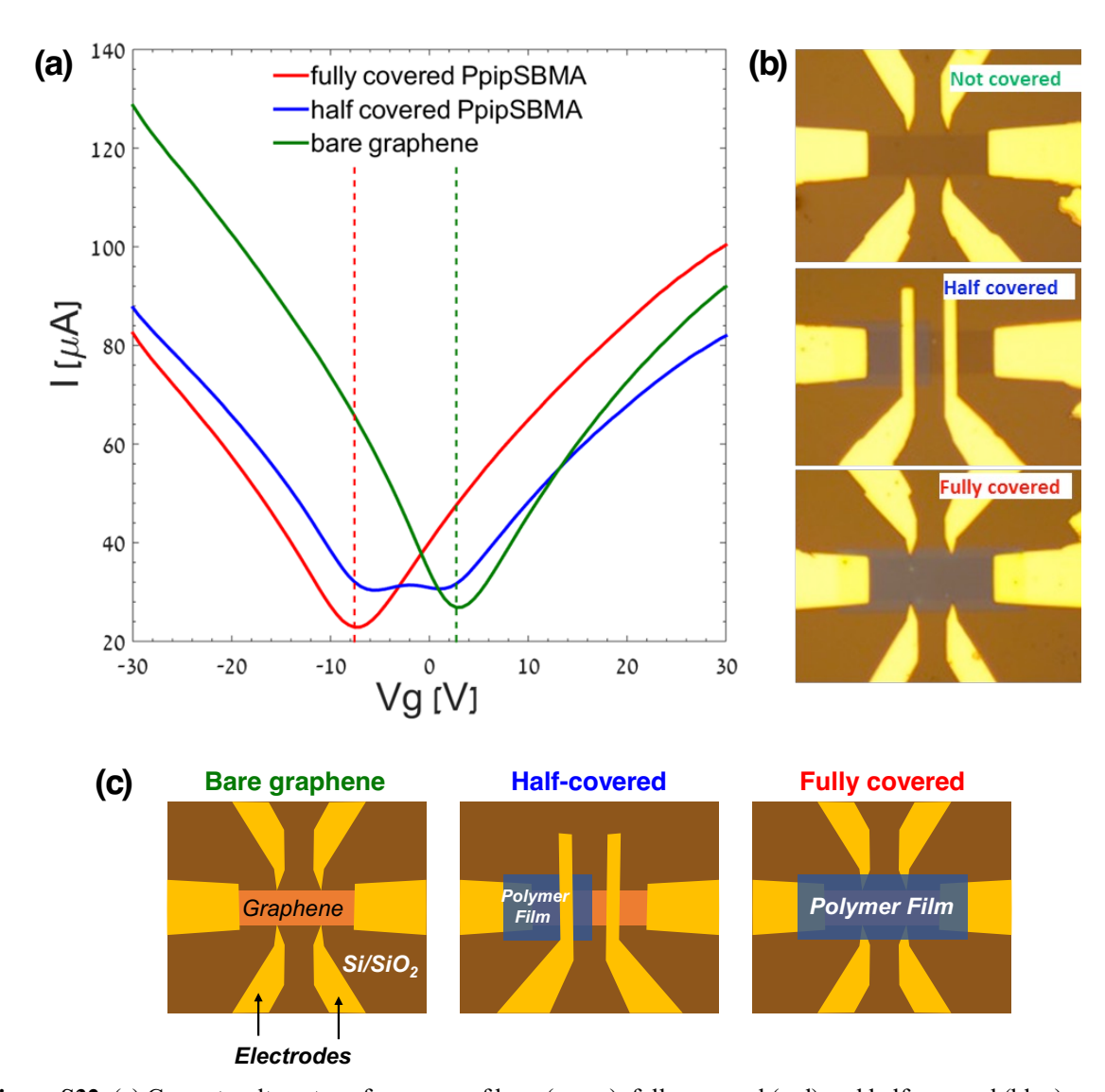


**Figure S32**. (a) Current-voltage transfer curves of bare (green), fully covered (red) and half-covered (blue) graphene field effect devices, (b) corresponding optical micrograph of the devices, and (c) schematic of fabricated devices for clarity.

# References

- (1) Wang, N.; Seymour, B. T.; Lewoczko, E. M.; Kent, E. W.; Chen, M.-L.; Wang, J.-H.; Zhao, B. Zwitterionic Poly(Sulfobetaine Methacrylate)s in Water: From Upper Critical Solution Temperature (UCST) to Lower Critical Solution Temperature (LCST) with Increasing Length of One Alkyl Substituent on the Nitrogen Atom. *Polym. Chem.* **2018**, *9* (43), 5257–5261.
- (2) Chang, C.-C.; Letteri, R.; Hayward, R. C.; Emrick, T. Functional Sulfobetaine Polymers: Synthesis and Salt-Responsive Stabilization of Oil-in-Water Droplets. *Macromolecules* **2015**, *48* (21), 7843–7850.
- (3) Hildebrand, V.; Laschewsky, A.; Päch, M.; Müller-Buschbaum, P.; Papadakis, C. M. Effect of the Zwitterion Structure on the Thermo-Responsive Behaviour of Poly(Sulfobetaine Methacrylates). *Polym. Chem.* **2016**, *8* (1), 310–322.

(4) Kim, J.; Hanna, J. A.; Byun, M.; Santangelo, C. D.; Hayward, R. C. Designing Responsive Buckled Surfaces by Halftone Gel Lithography. *Science* **2012**, *335* (6073), 1201–1205.